2

Electron Source

Contents

2.1 Introduction . . . 27
2.2 Polarized Electron Gun . . . 30
2.2.1 Specifications . . . 30
2.2.2 Design Philosophy . . . 32
2.2.3 Photocathode . . . 32
2.2.4 Polarization . . . 34
2.2.5 Vacuum and Mechanical Design . . . 35
2.2.6 Loadlock and Cathode Preparation Chamber . . . 35
2.2.7 Inverted Geometry Gun Tests . . . 36
2.2.8 Reliability . . . 36
2.2.9 Operation . . . 36
2.3 NLC Laser System . . . 37
2.3.1 Pump Lasers . . . 37
2.3.2 Ti:Sapphire Oscillator . . . 39
2.3.3 Pulse Shaping . . . 39
2.3.4 RF Laser Modulator . . . 39
2.3.5 Ti:Sapphire Power Amplifier . . . 40
2.3.6 Pulse Train Length, Intensity, Spot Size, and Steering Control . . . 41
2.3.7 Overall Technical Risks . . . 41
2.4 NLC Electron Injector Beam Dynamics . . . 41
2.4.1 NLC Injector Baseline Design . . . 41
2.4.2 Electron Gun Optics . . . 41
2.4.3 Intensity Jitter Limiting Aperture . . . 42
2.4.4 Bunching System . . . 43
2.4.5 Injector Linac . . . 47
2.5 Buncher Cavities . . . 51
2.6 Positron Drive Linac . . . 51
2.7 Diagnostics . . . 53
2.8 Operation . . . 56
2.8.1 Initial Set-up and Beam Maintenance . . . 56
2.8.2 Troubleshooting . . . 57
2.9 Conclusion . . . 57
2.A Polarized e^- Beam Photocathode RF Gun Development for the NLC . . . 58
2.A.1 Introduction . . . 58
2.A.2 Beam Dynamics . . . 59
2.A.3 Material and RF Considerations . . . 64
2.A.4 Laser System . . . 68

2.A.5 Integrated System . . . 73
2.A.6 Conclusions . . . 73
2.B Charge Limit and its Implications on High-Polarization Long-Pulse Charge 74
2.B.1 Introduction . . . 74
2.B.2 Generalization of CL Effect to Long-Pulse Operation . . . 74
2.B.3 Where We Are . . . 76
2.B.4 Cathode Improvements and Outlook . . . 77

2.1 Introduction

The electron injector for the Next Linear Collider (NLC) is based on the design of the injector for the SLC because many of the performance requirements for the NLC are similar to the SLC. The main difference is that the NLC injector has to deliver a train of bunches, therefore multibunch issues must be addressed.

The SLC polarized source which has operated so successfully since 1992, can be duplicated for the NLC with almost no changes to the polarized gun. We expect that the polarized source system will operate at better than 99% uptime efficiency based on the SLC experience. With ultra-high vacuum achieved in the SLC gun, the cathode lifetime has improved such that now it is greater than thousands of hours. Similar to the SLC, greater than 80% electron polarization will be achieved in the NLC. Some integrated experiments need to be performed to demonstrate that the polarized cathodes and cathode handling techniques available today can be applied to the cathode for the NLC polarized gun to achieve the required current for the NLC at greater than 80% polarization (Appendix 2.B).

There will be two electron injectors on the NLC: one for the collision and another for the positron-production electrons. The collision electron injector will have a polarized electron gun while the electron injector for positron production will have a thermionic gun. The injector for the collision electrons goes up to 2 GeV and has a lattice to match the beam into the linac-to-ring transition. The drive linac for the positron source goes up to 3.11 GeV in the first phase and 6.22 GeV in the second phase, and has the necessary optics to transport the beam to one of the two parallel beam lines for the positron production systems.

The low-energy transport portion of both electron injectors will be identical to provide operational flexibility and the flexibility of exchanging the thermionic electron gun for a polarized gun for future upgrades where two polarized electron sources are needed for $\gamma - \gamma$ collisions.

Figure 2-1 shows the injector for the collision electrons from the gun up to the linac to ring transition point. The bulk of this chapter addresses the collision electron injector beam line but Section 2.6 addresses the positron drive injector in as far as it is different from the collision electron injector.

The baseline approach for the NLC injector will be a conventional system with a DC polarized gun and bunching system. The conventional subharmonically bunching injector approach [James 1981] is a proven, mature technology, used on injectors around the world, including on the SLC. The polarized electron gun and laser system are similar to the one which has been very successfully and reliably used on the SLC.

Some differences in this system are necessary to provide for the long bunch train. The laser system will produce a 126-ns-long train of bunches which are nearly rectangular in shape with a full-width-half-maximum value of 700 ps, and 1.4-ns apart. The beam intensity at 80 MeV needs to be about $1.9 \times 10^{10} e^-$ in 22 ps for each bunch, an average pulse train current of 1 A. The rms intensity jitter needs to be within 0.5% integrated over the entire train.

The polarized source rf gun injector approach should be studied in parallel (Appendix 2.A) to take advantage of the extremely low emittances achievable with rf guns, but at this point the technology of producing polarized electrons with rf guns has yet to be developed and is not the baseline approach for NLC.

The injector described in this section is shown in Figure 2-1. Our goal is to design an injector beam line such that it can produce the required beam parameters for both NLC-I and NLC-II as shown in Table 2-1. It has a 120-kV DC polarized electron gun which needs to produce $2.8 \times 10^{10} e^-$ in each bunch for NLC-II. The gun will house a 3-cm^2 cathode. All the current SLC polarized guns have a 3-cm^2 cathode, though the original gun with a 2-cm^2 cathode has been used for SLC operation.

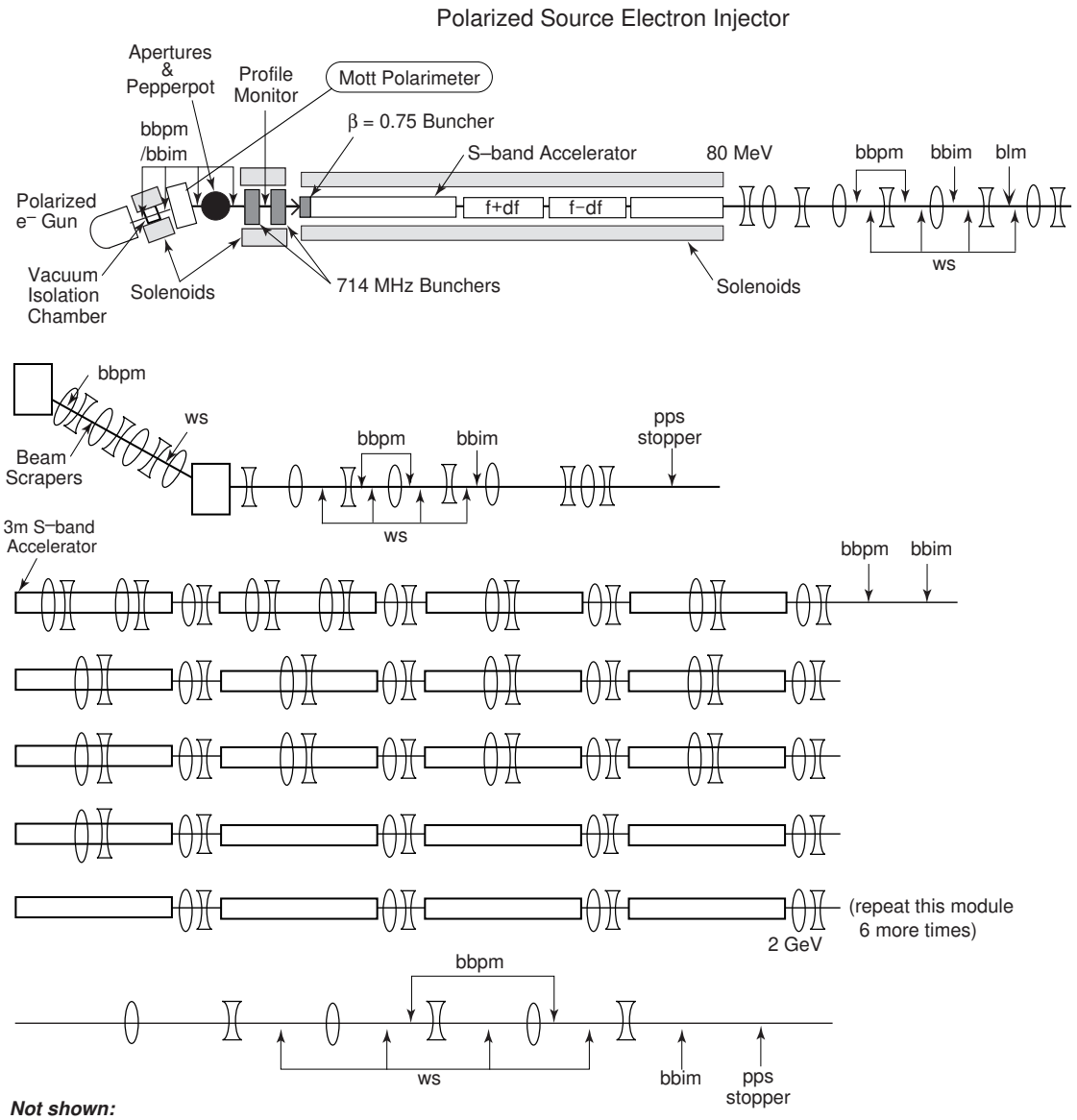

Figure 2-1. *2-GeV polarized electron source injector.*

A vacuum isolation chamber and a 20° bend protect the polarized electron gun from the downstream environment. The 20° bend also allows us to switch the beam into a Mott polarimeter station for occasional source polarization measurements. The train-to-train intensity jitter of the beam at the gun may be close to the allowed threshold of 0.5% due to the incoming laser intensity jitter on the photocathode. This will limit energy jitter in the linac to 0.25% as described in Chapter 1. An aperture 24-cm downstream of the 20° bend will be used to further reduce the electron beam intensity jitter of the bunched beam. Two 714-MHz standing-wave subharmonic bunchers and an S-band buncher-accelerator section compress the beam from the gun such that 83% of the charge is captured in 18° of S-band or 17.5 ps. PARMELA simulations were conducted from the gun through the second accelerator section, where the beam reaches 80 MeV ±0.6% in energy. This energy spread is for a single bunch not including the beam-loading effect due to the long bunch train.

Beam-loading effects in the subharmonic bunchers are mitigated by using cavities with low R/Q to minimize the beam loading and inject the beam during the fill time of the cavity. Axial magnetic field focusing will be used on the first two accelerator sections (up to 80 MeV) where the beam is expected to have a larger energy spread than in the rest of the injector linac. At 80 MeV, there will be an isochronous and achromatic bend to connect the low-energy beam line to the main injector beam line. This bend allows us to construct another low-energy injector line in the future which may be needed either for more reliability in the polarized source or possibly for the first polarized source rf gun injector for the NLC. There is a set of wire scanners on both sides of the achromatic bend to measure emittance of the beam from the low-energy beam line and the emittance going into the injector linac after the bend. In addition, the chicane will have a set of scrapers at the high-dispersion point to clip away tails which are not in the main bunch and a wire scanner following the scrapers to measure the energy spread. From 80 MeV up to 2 GeV, the linac will use 3-m accelerator sections and Δt method for beam-loading compensation. Each module will consist of four 3-m accelerator sections powered by 2 S-band Klystrons similar to the SLAC 5045 klystrons except for the slightly longer 4-μs pulse width. Quadrupole doublets between each section and some wrapped around the first few sections will be used to control the transverse dimension of the beam.

There are only a couple of technological-breakthrough issues associated with the baseline injector chosen for the NLC. We need to demonstrate in an R&D program that we are able to produce cathodes with the 80% polarization and the up to 3.2-A average current needed for NLC-II. Currently available photocathodes with 80% polarization and 3-cm^2 emitting area are capable of producing only one fourth as much charge as is required for NLC-I with the (Appendix 2.B). It would be important to develop an 80% polarization cathode that will produce at least the required charge for NLC-1. If such a cathode is not developed in time then it is possible to increase the charge by doubling the area of the cathode with some compromise to the beam emittance at the gun to produce at least half the required charge for NLC-1. Other options for increasing the charge from the cathode could include development of the gun technology such that higher electric field would be tolerable at the cathode.

The beam-loading compensation both in the subharmonic bunchers and in the injector accelerator need to be simulated in detail, and physically realizable cavities need to be designed for the bunchers and the accelerators. These technologies will be demonstrated in the Next Linear Collider Test Accelerator (NLCTA) injector upgrade.

The development of a reliable and stable polarized-source-rf-gun injector deserves a concentrated parallel effort in the laboratory. If it could be demonstrated that the polarized-source rf gun system with the much lower beam emittance can be reliably and stably operated, then it will simplify the damping ring design or at least make it easier to operate. If the demonstration programs prove successful, the polarized-source rf gun could become the baseline injector for the NLC in which case we might also use an rf gun for the positron drive injector to make it similar in operation to the collision electron beam line.

Parameters	NLC-I			NLC-II			Overhead	SLC
	A	B	C	A	B	C	20%	achieved
N/bunch at IP (10^{10})	0.65	0.75	0.85	0.95	1.1	1.25	1.5	
N/bunch at Gun (10^{10})	1.2	1.4	1.6	1.75	2.0	2.3	2.8	8.8
Iave at gun (A)	1.4	1.7	1.9	2.0	2.4	2.7	3.2	
N/bunch at intensity jitter aperture (10^{10})	0.95	1.15	1.3	1.4	1.63	1.85	2.2	
N/bunch at 80 MeV (10^{10}] in 18 ps	0.83	0.97	1.1	1.2	1.4	1.6	1.96	
Iave at 80 MeV (A)	0.95	1.11	1.26	1.37	1.58	1.8	2.2	
N/bunch at damping ring (10^{10})	0.75	0.88	1.0	1.1	1.28	1.45	1.7	5.5

Parameters	NLC Required	Simulation	SLC
			no train
Bunch train durations (ns)	126	126	
Bunch separation (ns)	1.4	1.4	
PW at the gun FWHM (ps)	700	700	2000
PWedge after bunching (ps)	18	18	18
ε n,rms at 40 MeV (10^{-4} m-rad)	1.0	0.5	1 to 1.3
$\Delta E/E_{edge}$ at entr. to DR. (%)	± 0.6	± 0.6	± 0.6 to 0.8
Train-to-train intensity jitter (%)	$<0.5\%$	negligible w/ intensity jitter limiting aperture	0.8 at gun 0.5 after bunching

Table 2-1. *NLC polarized electron source parameters up to the damping ring.*

2.2 Polarized Electron Gun

2.2.1 Specifications

The principal requirements of the polarized electron gun are given in Table 2-2. To achieve 1.5×10^{10} e^-/bunch at the interaction point (IP), about 2.8×10^{10} e^-/bunch or a peak current of 4.5 A must be extracted from the cathode. The maximum current that can be extracted is established by the space-charge limit of the gun. The gun will be designed for a space charge limit of 13 A at the operating voltage. Assuming adequate laser energy, the ability to extract high peak currents at a given voltage depends on the internal charge limit of the cathode, which in turn depends primarily on the success in achieving a negative electron affinity surface. Achieving a successful negative electron affinity surface requires an ultrahigh vacuum system with total system pressure $\leq 10^{-12}$ Torr (excluding H_2).

Field emission associated with a DC-biased cathode can be destructive to a negative electron affinity surface. Thus the average dark current should be 25 nA or less. To achieve this goal, the electric field on the cathode electrode surface should be kept below 7 MeV/ m at the operating voltage.

The intensity variations in the extracted electron pulse, including the jitter, are dominated by the properties of the laser pulse. On the other hand, the energy variations depend on the space-charge forces and the

Gun vacuum	$\leq 10^{-12}$ Torr (excluding H_2)
Operating voltage	120 kV
Cathode area	$3\,cm^2$
Extraction field	2.0 MV/ m
Maximum field on cathode electrode	<7 MV/ m
Space charge limit	13 A
Peak current at gun NLC I	2.5 A or $1.6 \times 10^{10} e^-$/bunch
NLC II	4.5 A or $2.8 \times 10^{10} e^-$/bunch
Number of bunches NLC I	90
NLC II	90
Bunch width at gun	700 ps FWHM
Bunch spacing	1.4 ns
Macropulse repetition rate NLC I	180 pps
NLC II	120 pps
Dark current	<25 nA DC
Intrapulse energy variation	≤1%
Gun normalized rms emittance	$< 5 \times 10^{-6}$ m-rad
Beam loss before bend	<0.1%
Cathode lifetime	≤200 h
Operating efficiency in any 1-week period	~98%
Polarization	≤80%

Table 2-2. *Gun specifications.*

properties of the high-voltage power supply system for biasing the cathode. The energy variation within the electron pulse should be ≤1%, and the intensity variation ≤0.5% at the gun.

As with the SLC source, it is assumed that if the normalized emittance of the electron beam at the gun is a factor of 10 less than that of the bunched beam, the bunched beam will not be affected by small changes in the gun emittance.

The 1/e decay rate of the quantum efficiency of the cathode should be ≥200 h to ensure a high-operating efficiency. The lifetimes may be a moot question if it is determined that the cathodes can be cesiated at the operating high voltage without damaging the surface of the semiconductor crystal. The cathode in the SLC gun has a lifetime >1000 hrs.

The electron beam should have the highest possible polarization, preferably >80%, while still meeting all other NLC specifications, in particular the intensity requirements. While the present-generation strained GaAs photocathodes used for the SLC have satisfactory polarization performance, they are incapable of generating the long, high-intensity bunch train required by the NLC owing to an inherent cathode charge limit phenomenon [Alley 1995]. A detailed description of the charge limit phenomenon, its implications on long pulse charge production, and the steps to be taken towards meeting the polarization and charge requirements of the NLC source are given in Appendix 2.B. The insufficient charge performance may be remedied by substantially increasing the doping density in the strained GaAs. Unfortunately, the increased doping density also degrades the beam polarization. Research is underway to develop a strained GaAs cathode capable of both >80% polarization and NLC charge production with reasonably sized cathodes.

2.2.2 Design Philosophy

Except for the issues associated with long pulse (on the order of 100 ns) operation, the SLC polarized electron source has been shown to meet the gun specifications given above. Thus it is planned to use much of the SLC-source design features for the NLC source. The features include an extremely good vacuum system to ensure long cathode lifetimes, use of a loadlock for installing and removing cathodes in the gun, and provision for testing backup cathodes and guns.

The SLC polarized electron gun with a loadlock will be the baseline design for the NLC source. Its performance and reliability have been well established with three years of smooth and nearly maintenance-free operation on the SLC. The "inverted-geometry" gun, which has a grounded body, will be considered as a logical upgrade if it is proven to be as reliable as the SLC gun. This gun has the advantage of being more compact with a simplified high-voltage operation, but it requires more testing in an accelerator environment. The cross sections of the SLC gun and the inverted-geometry gun are shown in Figures 2-2 and 2-3. The beam characteristics for the two guns are essentially identical because of similar focusing electrode design and the use of identical beam optics components. Both types of guns are configured to use the same gun support bench and will mate the downstream beam line in an identical manner. Therefore, switching between the two types of guns is as easy as switching between two guns of the same type, which should take about one day.

The preparation of photocathodes for polarized guns is a highly sophisticated operation that is not compatible with the accelerator environment. Thus it is necessary to have a cathode preparation laboratory that is separate from the accelerator. The preparation laboratory will be equipped with an ultrahigh vacuum (UHV) cathode test system capable of measuring the polarization as well as the quantum efficiency of a cathode sample at low voltage. Cathodes prepared in this laboratory for either the NLC operating source or the spare will be transported under vacuum.

Additional facilities, including certified clean rooms, will be necessary for the assembly and repair of guns.

2.2.3 Photocathode

Due to their superior polarization performance, photocathodes of strained GaAs epitaxially grown on GaAsP will be the primary candidates for use on the NLC. As is discussed in Appendix 2.B, the intrinsic charge limit effect inherent in p-type negative electron affinity semiconductor photocathodes may lead to inadequate charge performance for the NLC bunch train, from SLC-type uniformly doped strained GaAs cathodes with >80% polarization. However, there is room for significant improvement on the photoemission characteristics for such cathodes. More cathode research and development is expected to yield high-polarization, high-intensity cathodes that will meet the NLC requirement.

Conventional cathode preparation requires heat cleaning at 600°C for 1 hour. This high temperature results in some unwanted reconstruction at the surface. In addition, providing the high temperature in an UHV system places a definite limit on the reliability of the system due to the possibility of cathode contamination during the accompanying high pressures, and also because of the high potential to open a vacuum leak. Several techniques for low-temperature cathode preparation are being explored, including capping (following fabrication of the cathode) with a low-temperature protective layer, and cleaning at low temperature in a cathode preparation chamber using an atomic hydrogen (H^*) beam.

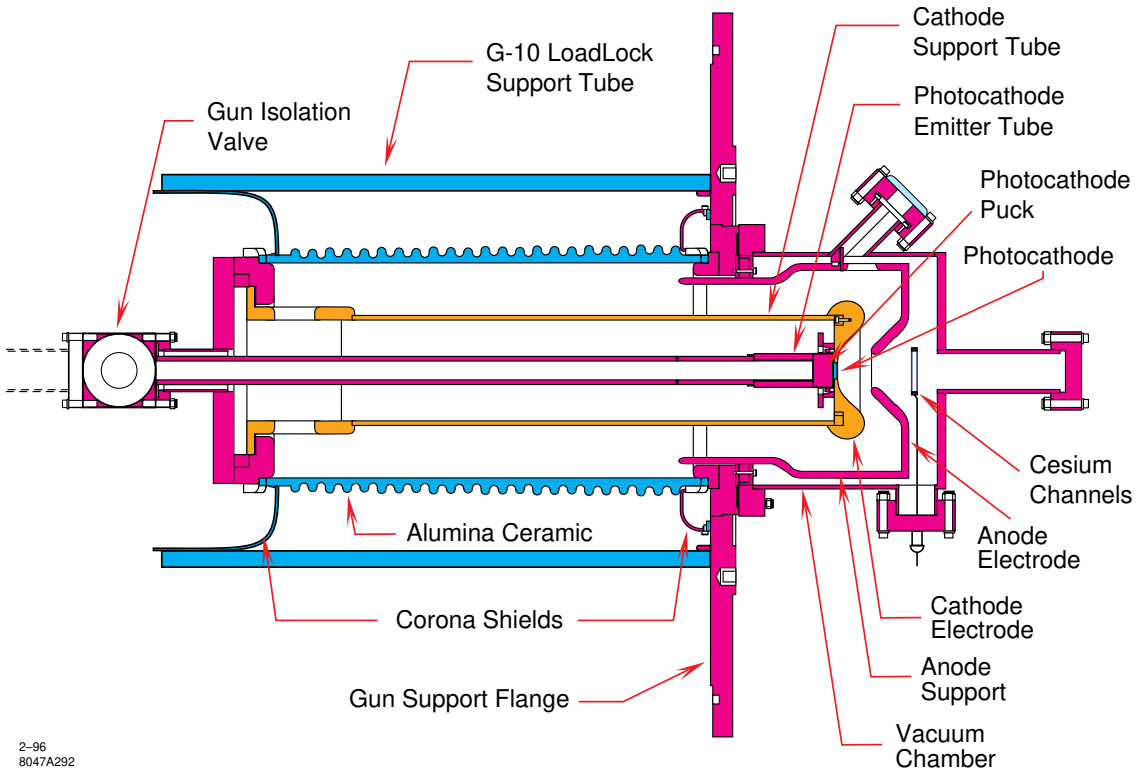

Figure 2-2. *Cross section of the SLC polarized electron gun (loadlock not shown).*

Reducing the dark current in the SLC source to <50 nA has usually been difficult to achieve. Ultrahigh-purity water cleaning techniques now under investigation may make it easier to achieve the low levels of dark current desired for the NLC. It is possible to use a pulsed high-voltage cathode bias if necessary.

As described in Appendix 2.B, a successful low-temperature heat-cleaning technique will allow operation with a cathode having high-dopant density at the surface. Such a cathode may greatly increase not only the cathode charge limit, but also the quantum efficiency (QE) achievable when cesiating. With high initial QE achieved with the high dopant density, and long lifetimes achieved by having a clean UHV system and low dark current, it should be possible to operate the NLC source for many days without recesiating. The SLC has already demonstrated that such sources can operate continuously for many months without cathode maintenance other than recesiation. A recesiation, which takes 15 to 30 minutes, can be done by machine operators through the computer control system. The interval between cesiations on the SLC is about one week and it gets longer as the gun remains under vacuum.

The quantum efficiency decay rate, that is, the cathode lifetime is an important operating parameter. Lifetimes of over 1000 hours have been achieved with the SLC. A lifetime of 200 hours corresponds roughly to a drop of 10%/day in the value of the QE.

Other types of photocathodes are being investigated in various laboratories around the world including SLAC. The gun can accommodate any of these if they should prove superior to the SLC cathodes. A fundamental requirement for choosing a new type of photocathode material is that the polarization of the electron beam should be at least as high as the highest achieved in SLC with the GaAs-GaAsP strained

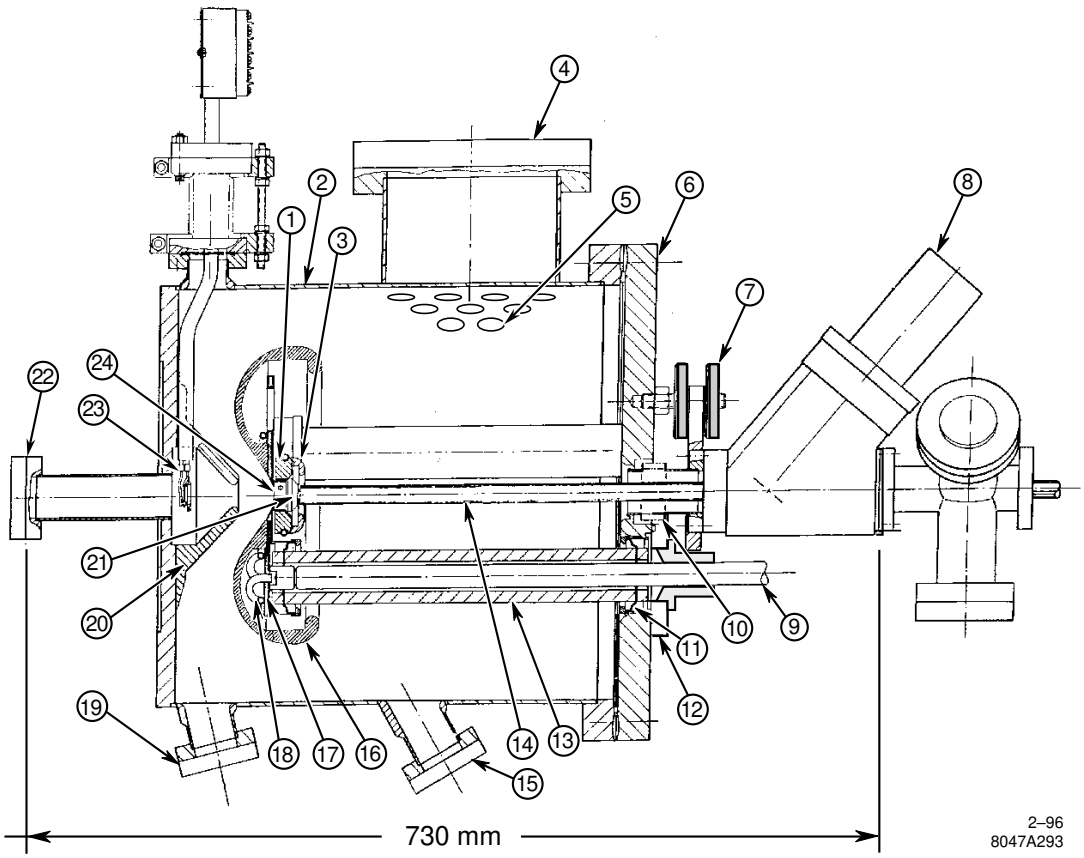

Figure 2-3. *Cross section of inverted gun: (1) docking mechanism and puck holder, (2) gun body, (3) shielding rings, (4) ion pump port, (5) pumping holes, (6) end flange, (7) jacks, (8) access valve, (9) high-voltage cable, (10) bellows, (11) Kovar weld ring, (12) gas seal flange, (13) ceramic insulator, (14) transporter rod (only in place while changing cathode), (15) Viewing port, (16) cathode electrode, (17) support plate, (18) gas tubes, (19) illumination window, (20) anode electrode, (21) puck, (22) exit port to beam line, (23) cesiator, (24) photocathode.*

lattice cathodes, and the charge limit associated with the cathode must not prohibit achievement of the desired electron intensities. In addition, there must be a source laser capable of producing the required energy at the wavelength that provides the highest polarization.

2.2.4 Polarization

The polarization of the electrons extracted into vacuum from the 100-nm SLC strained-lattice photocathodes is about 80% for the high peak intensity SLC pulses, and about 85% for very low intensity pulses for which the cathode QE can be very low. The effort to improve the GaAs-GaAsP cathodes is aimed at producing cathodes with greater than 80% polarization at NLC beam intensities with moderate-sized (3 to 9-cm^2) cathodes.

The polarization of the NLC cathodes during full current extraction must be tested for each cathode crystal before it is installed at the injector. To perform such tests, a Mott polarimeter and spin rotator, optimized for the operating energy of the NLC source, will be an integral part of the source. The Mott polarimeter will be calibrated against a polarimeter known to have an absolute accuracy of 1% or better.

There are conditions at the source that can change the polarization of the electron beam slightly. Thus, as a diagnostic the operating source as well as the development system will be equipped with a Mott polarimeter as shown in Figure 2-1.

2.2.5 Vacuum and Mechanical Design

To achieve the desired high-voltage performance, it is critical to minimize field emission from the surface regions that see high electric fields. Extremely careful attention will be given to the fabrication of the cathode and anode electrodes and the cleanliness of all surfaces exposed to the gun vacuum. The electrodes will be fabricated using stainless steel with low carbon content and low inclusion density. The machined electrodes will be polished with diamond paste to a 1-mm finish with zero tolerance on visible pits and scratches. All components that operate at high voltage will be flushed with high-purity water before final vacuum firing. The assembly and alignment of the gun vacuum components will be done in a Class 100 clean room to avoid air-borne contamination.

Both ion pumps and nonevaporable getter (NEG) pumps will provide the pumping power for all gas species with the exception of inert gases. A high-sensitivity residual gas analyzer (RGA) will be used to monitor the gun vacuum. Following assembly, the gun is to be baked until the room temperature vacuum is $\sim 10^{-12}$ Torr excluding H_2.

The conductance between the gun chamber and the injector where the vacuum is significantly poorer will be minimized by a vacuum isolation chamber characterized by limited aperture conductance and extremely high pumping speed. A modest bend of 20° after the vacuum isolation chamber will further isolate the gun vacuum system and prevent back-reflected electrons from hitting the cathode or induce gas desorption near the cathode.

To attain the desired high-voltage performance, the gun must be high-voltage processed following the vacuum bake to eliminate field emission spots on the cathode electrode surfaces. This process involves gradually increasing the voltage in the presence of a low pressure of N^2 if necessary—until the dark current at the operating voltage is well below 25 nA.

2.2.6 Loadlock and Cathode Preparation Chamber

While the gun provides a vehicle for extracting high-intensity electron beams from a photocathode and at the same time providing the necessary UHV conditions required for reliably operating a negative electron affinity photocathode, its functionality is fully realized only with the help of a loadlock and a cathode preparation chamber. The preparation chamber is a UHV system in which a cathode is prepared to have an negative electron affinity surface, while the loadlock allows the cathode to be installed in and removed from the preparation chamber and installed in the gun itself without breaking vacuum in either system.

Since the cathode preparation is time consuming, taking about 8 hours and even longer when using a loadlock, it is best done in a chamber separate from the gun. The necessary cleaning techniques and the recipe for applying Cs_2 and an oxide are well established.

2.2.7 Inverted Geometry Gun Tests

The prototype inverted structure gun at SLAC will be extensively tested to ensure it can match the SLC photocathode gun for good cathode performance. Based on the results of these tests, the details of the NLC gun upgrade design will be determined.

2.2.8 Reliability

Based on the SLC experience, it is believed that achieving near 100% operating reliability over a period of several years of continuous operation is possible. The provisions to be incorporated into the NLC source to ensure this result are:

- Use of a loadlock system to insert and remove cathodes into the gun without breaking the gun vacuum.
- Possibly using a double-gate valve for connecting the gun to the loadlock to reduce the chance of vacuum contamination of the gun should one gate valve fail.
- A vacuum isolation/differential pumping section downstream of the gun to protect it from the poorer vacuum system of the injector.
- Provision for a spare polarized electron source for completely testing cathodes for intensity, lifetime, and polarization.
- Provision of a transfer system for moving cathodes under vacuum between the NLC source, the spare source, and the cathode activation chamber.
- Provision of spare guns and spare cathode activation chambers.

2.2.9 Operation

Following the SLC experience, it is possible for the accelerator operators to remotely monitor and perform routine maintenance on the polarized electron source through a computer control system. For this purpose, the following displays will be available to the operators:

- The full residual gas spectrum of the gun and downstream vacuum systems.
- The transverse and longitudinal shape of the electron pulse at the gun.

A complete set of analog and digital signals will be available to the operators. These signals will also be history-buffered. The analog data will be collected locally for each pulse over the last few-minute period.

A representative value of the data will be history-buffered unless the system indicates a problem, such as a vacuum burst, in which case data will be recorded for every pulse. The principle operational task for the operator is to periodically cesiate the cathode. As the SLC has thoroughly demonstrated, this process can be fully automated (but initiated by operator command).

2.3 NLC Laser System

The NLC laser requirements are driven by the requirements on the electron beam from the polarized source photocathode [Alley 1994]. The most important of these requirements are the polarization and the charge limit properties of the GaAs cathodes. The laser wavelength needed varies with different cathode types and is chosen to maximize these parameters. Thus a range of wavelengths from 760 to 890 nm is needed. A quantum efficiency of 0.1% is assumed for the cathode based on the SLC experience. Electron beam optics considerations determine the other properties of the laser system such as longitudinal and transverse shape, stability, and so on.

The proposed NLC laser system uses Titanium-doped sapphire (Ti:Sapphire) as the primary laser material. Pumping of the Ti:Sapphire is provided by a pair of commercial Nd:YAG lasers. Overall macropulse optical shaping is performed with an electronic feedback driving a Pockels cell attenuator. Micropulse shaping and selecting is done with a series of resonant Pockels cells. All of the technology used is fairly conventional, although the resulting system is somewhat complex. A schematic of the laser system is shown in Figure 2-4. The laser system is expected to meet the following specifications:

Wavelength	760 to 890 nm
Polarization	$> 99.7\%$
Bunch train length	Up to 150 ns
Bunch spacing	714 MHz, 357 MHz or 178.5 MHz
Bunch width	< 1 ns as close to rectangular as possible.
Pulse contrast	$<$ 5:1000 for the 714 MHz spacing, more is tolerable for the 357 and 178.5-MHz spacing.
Spot size on the cathode	Variable from 10 to 20-mm in diameter.
Transverse uniformity	As close to rectangular as possible.
Bunch energy	20 mJ
Bunch train energy stability	0.5% rms
Repetition rate	180 Hz

2.3.1 Pump Lasers

The pump laser system is required to produce a total of 150 mJ, 180 Hz, at approximately 500-nm wavelength. This can be done using two commercial Q-switched frequency-doubled Nd:YAG lasers. We have chosen to use two Coherent Infinity YAG lasers. These lasers use a seed laser and a phase conjugate amplifier configuration to obtain good transverse mode quality at high repetition rates. The two pump lasers are each operated at 90 Hz, and interleaved to obtain the required 180-Hz output.

Beam interleaving is achieved by rotating the polarization of one of the pump lasers and then combining them with a polarizing splitter/combiner. A pulsed Pockels cell is used to control the polarization of the

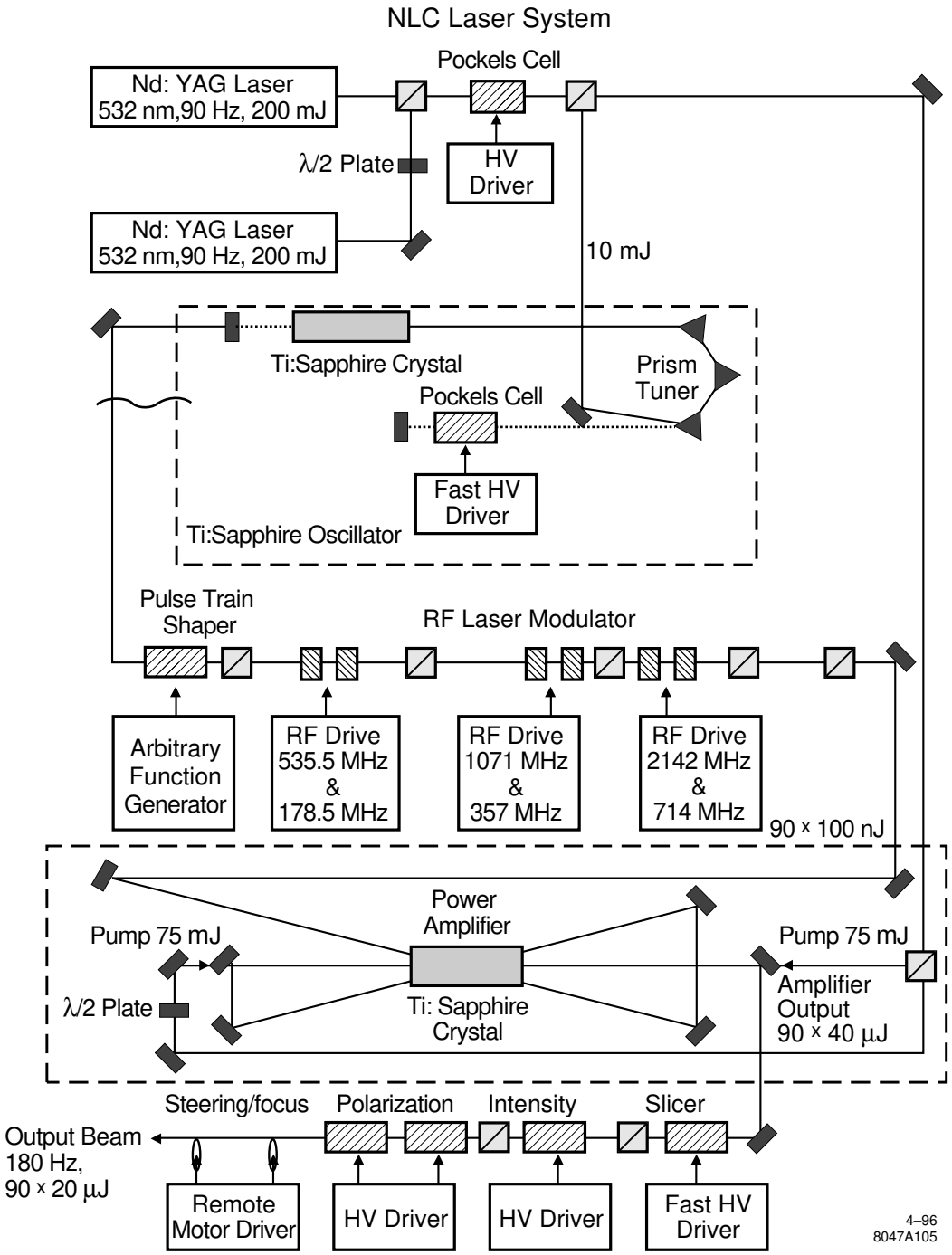

Figure 2-4. *Schematic diagram of the NLC polarized source laser system.*

combined pump beam. A waveplate is used to adjust the splitting ration between the oscillator and amplifier. A second waveplate and polarizer is used to adjust the pump energy to each end of the amplifier.

2.3.2 Ti:Sapphire Oscillator

The oscillator produces a long (~150 ns) optical pulse with approximately 1 mJ of energy. Wavelength tuning is accomplished with a series of Brewster angle prisms (birefringent tuners would also work). A Pockels cell and the S-polarization loss of the prisms are used to Q-switch the cavity. The resulting output pulse is later chopped to produce the required pulse structure.

The primary source of output fluctuation in this system are changes in pump laser energy changing the output pulse energy and timing (due to changes in gain). The timing changes, coupled with the pulse chopping, produce additional intensity fluctuations. We plan to use a feedforward system which, on each pulse, adjusts the Q-switch time for the Ti:Sapphire laser to compensate for changes in the pump energy. If the system detects a high energy pump pulse, it delays the Q-switch time to compensate for the decreased build-up time (due to higher gain). The system is adjusted to slightly under-compensate for the gain change, the resulting slight timing shift (of the Q-switched pulse, not the output) compensates for the changes in Q-switched pulse energy.

A system of this type is used on the SLC source laser to provide an output with intensity fluctuations of <1% rms (0.6% has been demonstrated) with pump fluctuations of >3% rms. The limiting factor here is the stability of the pump laser intensity. We believe this technology can be improved to reduce output fluctuations to <0.5% rms (with expected pump fluctuations of <2% rms) and to improve the feedforward system.

All the oscillator components are commercially available. With the exception of the intensity stability, the required output parameters should be obtainable using conventional technology. The intensity stability should be obtainable with a modest extension of the feedforward technology used at SLAC.

2.3.3 Pulse Shaping

The pulse shaper uses an arbitrary function generator and a fast (10 ns) high-voltage (5 kV) amplifier driving a Pockels cell to shape the output pulse. The final electron beam pulse train shape will be measured and a software feedback will be used to control the function generator. The Pockels Cell are commercially available. The high-voltage driver is similar to units developed at SLAC for other laser projects.

2.3.4 RF Laser Modulator

The NLC requires a train of bunches about 1-ns wide, nearly square in shape, and 1.4-ns apart. In addition, the option of running with a 2.8 or 5.6-ns bunch separation is also desired. The laser system will use a series of rf-driven resonant Pockels cells to produce the required pulse shape. Two rf-driven Pockels cells at $f_1 = 714\,\mathrm{MHz}$ and $f_2 = 2142\,\mathrm{MHz}$ in series and a polarizer will produce an optical train according to the equation $OT_{1.4} = A \sin^2[\sin(\omega_1 t - \pi/4) + 0.2\sin(\omega_2 t - 3\pi/4) + \pi/4]$ which is a train of nearly square pulses 1.4-ns apart and 1-ns wide as illustrated in Figure 2-5. To produce the 2.8-ns pulse separation, this system

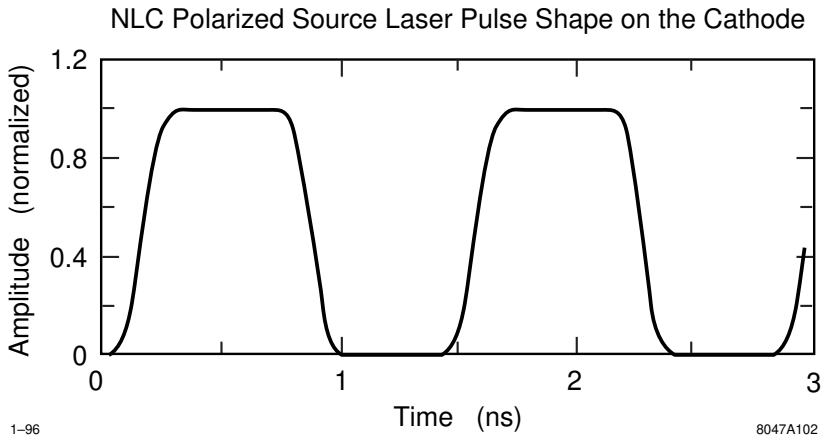

Figure 2-5. *NLC polarized source laser pulse shape at the cathode.*

of Pockels cells and polarizer is used in series by two other Pockels cells at $f_3 = 357\,\mathrm{MHz}$ and $f_4 = 1071\,\mathrm{MHz}$ and a polarizer, and for the 5.6-ns bunch separation, an additional pair of Pockels cells at $f_5 = 178.5$ and $f_6 = 535.5\,\mathrm{MHz}$ and a polarizer is used. Thus, the equation for the train of bunches separated by 5.6 ns is the product of the output of each of the pair of Pockels cells and polarizer systems:

$$\begin{aligned} \mathrm{OT}_{5.6} = \quad & \mathrm{A}\sin^2[\sin(\omega_5 \mathrm{t} + \pi/16) + 0.2\sin(\omega_6 t + 3\pi/4) + \pi/16]^* \\ & *\sin^2[\sin(\omega_3 \mathrm{t} + \pi/8) + 0.2\sin(\omega_4 t + 3\pi/8) + \pi/4]^* \\ & *\sin^2[\sin(\omega_1 \mathrm{t} - \pi/4) + 0.2\sin(\omega_2 t - 3\pi/4) + \pi/4] \end{aligned} \tag{2.1}$$

The laser intensity between the main pulses is almost completely quenched and the area of the residual pulse between the main pulses is 0.2, 0.5, and 1.4% of the main pulse for the 1.4, 2.8 and 5.6-ns separation cases, respectively. It is expected that most of this charge produced between the main pulses will be lost early in the injector beam line due to its poor bunching and matching into the lattice, as compared to the main bunch.

If standard KDP Pockels cells are used, a peak rf voltage of approximately 5 kV is required. With a resonant circuit Q=100, the required drive power is approximately 3 kW peak (<1 W average).

2.3.5 Ti:Sapphire Power Amplifier

The power amplifier operates in a 3-pass "bow tie" configuration with a gain of 10 each pass. A fairly conservative amplifier efficiency of 5% is assumed. Both ends of the laser rod are pumped to reduce the possibility of damage from the pump laser energy density. The required pump energy density of approximately $2\,\mathrm{J/cm^2}$ is within the limits for continuous operation. The average pump power to the crystal is approximately 30 W, well within the thermal fracture limit for Ti:Sapphire. The Ti:Sapphire thermal fracture limit is 5 times more than for the YAG [Wanant 1994], the YAG limit is $30\,\mathrm{W/cm^2}$, [Koechner 1992], and the spot size on the cathode is 2 to $3\,\mathrm{cm^2}$.

The feedforward system used in the oscillator can also compensate for changes in the gain of the amplifier. This should permit operation at the required 0.5%-rms output stability.

2.3.6 Pulse Train Length, Intensity, Spot Size, and Steering Control

The train of pulses from the amplifier is sliced to the desired overall length with a fast, high-voltage driver and a Pockels Cell. This system will probably have rise and fall times of approximately 5 ns. Faster pulses may be possible, but some high-voltage driver development would be required. The output intensity is controlled by a high-voltage amplifier driving a Pockels cell.

The output polarization is switched using two Pockels cells and high-voltage driver. Laser circular polarizations >99.7% are easily obtainable. Electron polarization measurements can be used to optimize the drive voltage on the Pockels cells to eliminate any birefringence in the transport line to the photocathode.

The beam spot size and position on the photocathode can be controlled with a remotely actuated telescope.

The propagation path and optics of the laser will be determined by the geometry of the physical layout of the injector with respect to the laser and is straightforward.

2.3.7 Overall Technical Risks

The most challenging requirement for the laser system is the output intensity stability. It is believed that this can be met with the use of feedforward system. The rf laser modulation is in principle straightforward, but some development may be required to obtain the required electrical Qs for the Pockels cells. The transverse mode structure from the output of the amplifier is difficult to predict. With the addition of spatial filtering, it should be possible to produce a good transverse-mode beam. In general, development of this laser system is anticipated to require approximately three man years.

2.4 NLC Electron Injector Beam Dynamics

2.4.1 NLC Injector Baseline Design

As shown in Figure 2-1 and discussed in Section 2.1, the NLC injector is like the conventional injector used on the SLC with a DC high-voltage gun and subharmonic bunching system. In this section we describe the beam dynamics from the gun through the injector linac.

2.4.2 Electron Gun Optics

The plan is to use a modulated laser to extract an electron bunch train from the photocathode. The electron beam energy from the gun will be 120 keV, a comfortable operating point for the polarized electron source. The proposed gun for the NLC polarized electrons has a large, 3-cm^2 cathode. The electrodes are shaped to minimize emittance for operating bunch currents and reduce the electric field gradients near the cathode to avoid arcing in this region. We used EGUN to simulate the beam from the gun. Figure 2-6 shows the ray-trace of the beam from the cathode to 12-cm downstream. The normalized edge emittance is 5.6×10^{-6} m-rad and the beam envelope radius is 1.2 cm at the tip of the anode.

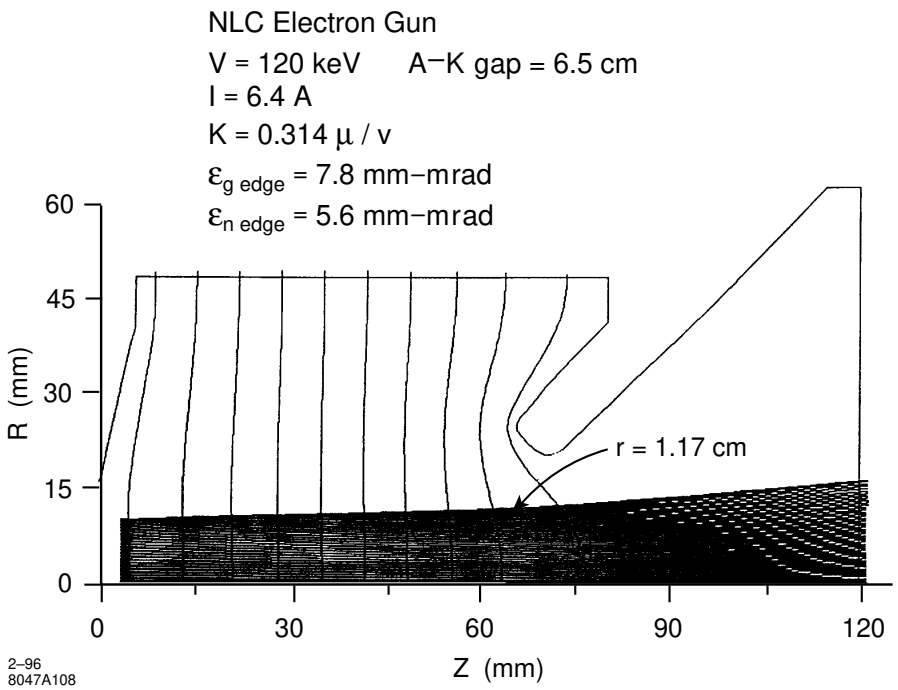

Figure 2-6. *Ray trace of the NLC electron beam from the gun.*

2.4.3 Intensity Jitter Limiting Aperture

A scenario for reducing the electron intensity jitter is to locate a fixed aperture in the 120-keV beam line at a location where the beam size is proportional to space charge. With this method, we hope to reduce the intensity jitter by scraping more charge when more charge is produced at the gun and less charge when less charge is produced at the gun. For the proposed NLC injector design, such a location exists 24-cm downstream of the 20° bend. Using a 1.25-cm aperture, we can reduce a 2% intensity jitter at the gun to be immeasurable in the bunched beam, while losing 17% of the charge in the aperture. Since this loss occurs after the gun vacuum isolation chamber and the 20° bend, it should not cause any damage to the photocathode based on various gun test experiences on the SLC polarized source. Figure 2-7 shows the correlation of charge per bunch in the downstream part of the injector with the charge produced at the gun. Figure 2-8 shows the charge in 18 ps at 80 MeV with and without the aperture. Notice that without the aperture the correlation has about a 45° slope, while with the appropriate aperture the slope is greatly reduced for the bunched beam intensity.

Studies were conducted to see how sensitive this scheme is to the location of the aperture along the beam line and to various nominal charge intensity scenarios. To study the effect of the criticality of the location of the aperture it was moved in simulations by ±2 cm from the nominal location and no observable difference in the performance of the aperture was detected. Reducing the nominal operating intensity to 3/4 or 1/2 of the nominal charge has a measurable effect on the aperture size needed for reducing the intensity jitter. At 3/4 charge, an aperture 1.5-mm smaller in radius is needed and at 1/2 charge, another 1-mm smaller is needed. To accommodate the changes in the operating intensity from the gun, the aperture would have to be mechanically designed such that its size can vary in small increments of less than 1 mm.

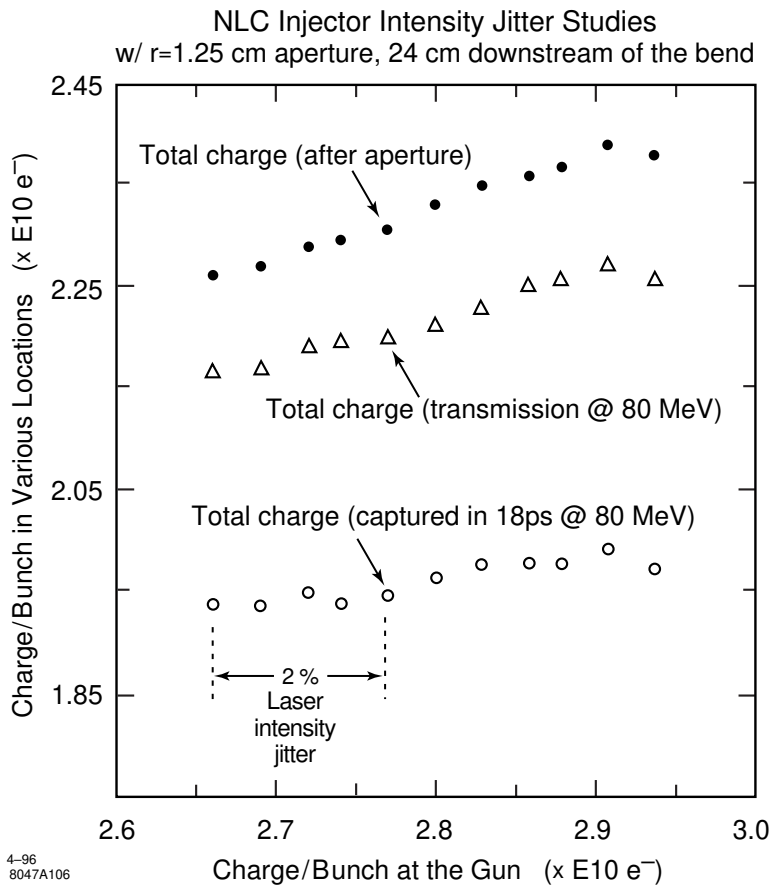

Figure 2-7. *NLC injector intensity at various locations as a function of charge from the gun going through a fixed aperture after the 20° bend near the gun.*

2.4.4 Bunching System

As shown in Figure 2-1, two 714-MHz standing wave subharmonic bunchers are located 74-cm apart downstream of the intensity jitter limiting aperture. The S-band buncher is a four-cavity, $\beta = 0.75$ traveling-wave section and is located 42-cm downstream of the second subharmonic buncher. Immediately following the S-band buncher is a $\beta = 1$, 3-m S-band accelerator section which acts as a further buncher in the first meter. This bunching system compresses the beam such that 83% of the in-coming charge is captured in 18° of S-band or 17.5 ps. Given that 17% of the beam is lost in the intensity limiting aperture, for $2.8 \times 10^{10} e^-$ per bunch at the gun we expect to have $1.96 \times 10^{10} e^-$ in 18 ps per bunch after bunching. PARMELA simulations were conducted from the gun to the end of the second accelerating section where the beam energy is 80 MeV±0.6%. Figure 2-9(a), (b), (c), and (d) show the single bunch charge distribution profile in time, transverse particle distribution, longitudinal particle distribution, and the energy spread profile, respectively, at the end of the second accelerator section.

At the end of the second accelerator section the beam-normalized rms emittance is 4.5×10^{-5} m-rad. Figure 2-10 shows the normalized rms emittance from the gun up to the end of the second accelerator section and Figure 2-11 shows the beam edge envelope.

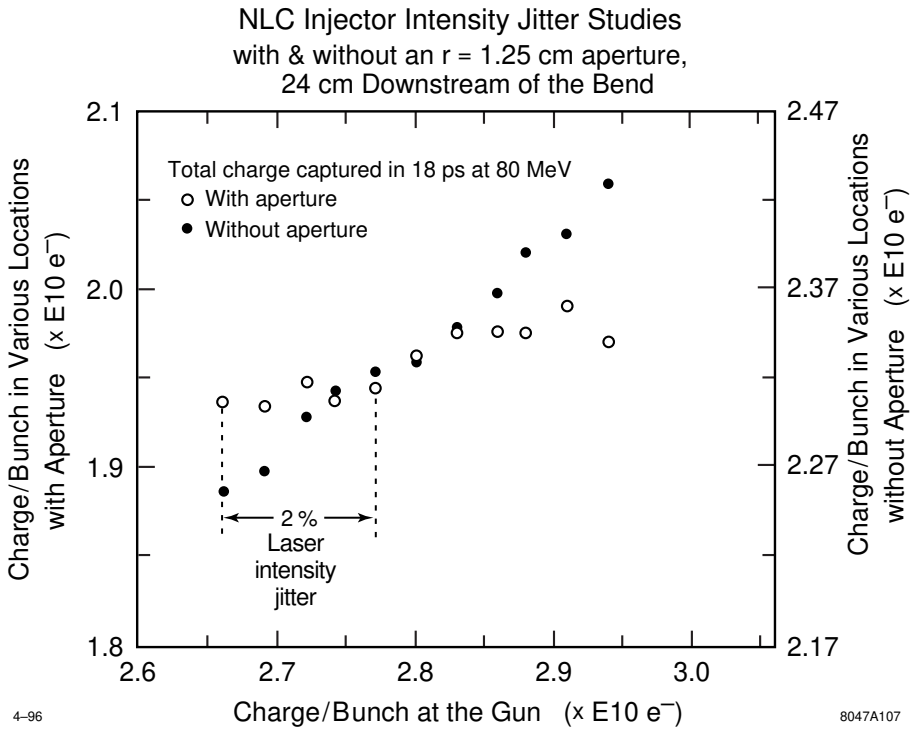

Figure 2-8. *NLC injector intensity after bunching as a function of charge from the gun with and without an aperture after the bend.*

Beam loading in the subharmonic bunchers is minimized by judiciously choosing a low $R/Q \sim 10\Omega$, a high Qo ~10000, and a coupling coefficient of $\beta = 1$, we can force a low beam-induced voltage and a long filling time of the cavity, thus minimizing the effects of beam loading in it. The fill time in this case will be 2.2 μs, much greater than the 126-ns bunch train length.

Since 17% of the charge is intercepted by the intensity jitter limiting aperture for the highest charge operating scenario, with 4.5 nC from the gun there will be 3.7 nC at the first subharmonic buncher and with a 700-ps bunch length it will occupy 180° of the 714-MHz subharmonic buncher rf. The beam-induced voltage in the first subharmonic buncher by the time the ninetieth bunch goes through will be:

$$\mathrm{Vb1} = [0.5q(R/Q)\omega/\pi] \times 90 \text{ bunches} = 3.7\,\mathrm{nC} \times 10\omega \times 714\,\mathrm{MHz} \times 90 = 2.4\,\mathrm{kV} \quad . \tag{2.2}$$

For the second subharmonic buncher, the bunch length is more like a δ function and

$$\mathrm{Vb2} = [0.5(R/Q)\omega] \times 90 \text{ bunches} = 3.7\,\mathrm{nC} \times 10\omega \times \pi \times 714\,\mathrm{MHz} \times 90 = 7.5\,\mathrm{kV} \quad . \tag{2.3}$$

Bunching simulations indicate that we need 18 kV in the first subharmonic buncher and 34 kV in the second for optimum bunching for the highest charge scenario. Since the centroid of the bunch is at about 90° ahead of the crest, the induced phase change in the first subharmonic buncher will be arctan(2.4/18) ~8° and in the second arctan(7.5/34) ~12°. This phase shift is not negligible and needs to be compensated. We plan to drive the cavity with as much power as would be needed to compensate for the voltage induced by the beam in the steady state plus the voltage needed for optimum bunching, and then inject the beam during the fill time of the cavity when the voltage in the cavity reaches the voltage needed for optimum bunching. At the time of beam injection, the phase of the generator power must be shifted by the amount that would be induced by the beam in the steady state.

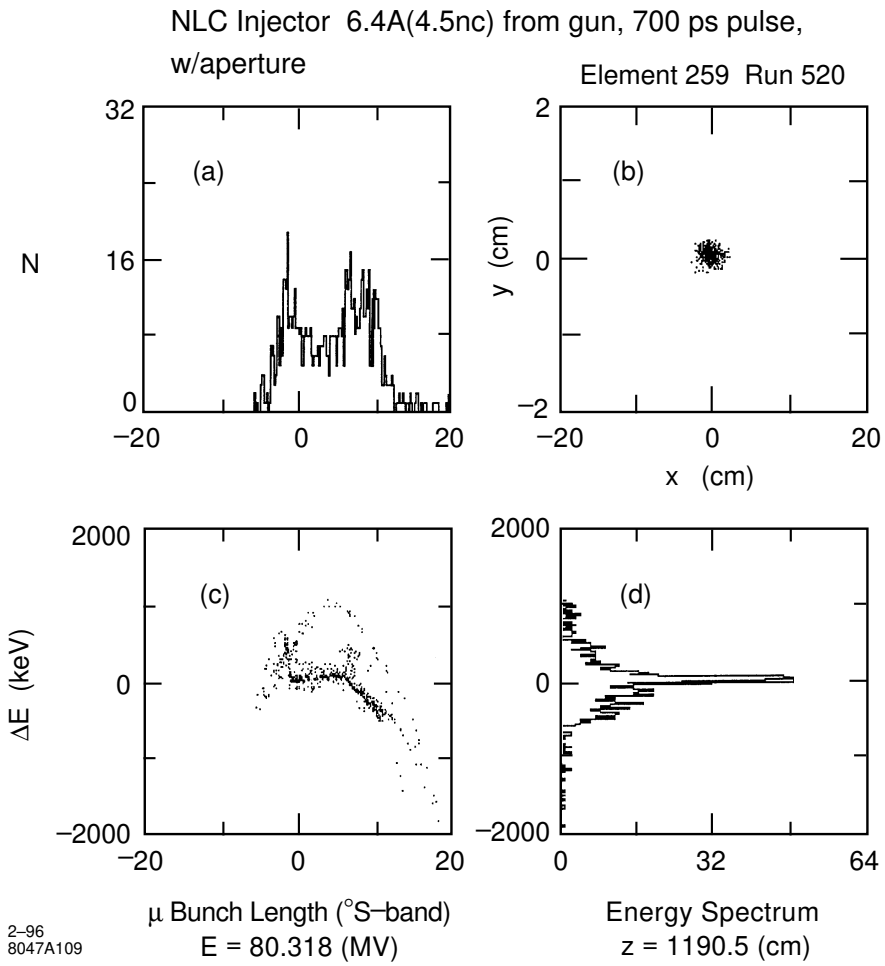

Figure 2-9. *PARMELA results of beam longitudinal and transverse distribution at the end of the second accelerator section. (a) bunch shape, (b) transverse distribution, (c) longitudinal distribution, (d) energy spread.*

The average current in the bunch train is 3.7 nC/1.4 ns= 2.6 A. The steady-state beam loading in the first subharmonic buncher where the beam occupies 180° of the rf, is $(1/2) \times \mathrm{Ib} \times (R/Q) \times Qo/(1+\beta) = 65\,\mathrm{kV}$. The generator power needed for bunching and beam-loading compensation is 42.3 kW. For a beam which is at 90° ahead of the crest, the steady-state phase shift is $\arctan(\mathrm{Vbs/Vg}) = \arctan[65/(18+65)] = 38°$, where Vbs is the steady-state beam induced voltage, and Vg is the generator voltage. Thus, at the time of the beam injection, the generator power is shifted by 38°, which is felt by the cavity at the fill rate. By the time the entire bunch train goes through the cavity, the generator voltage felt by the cavity is only 2.3 kV with an 8° phase shift, exactly what is needed to compensate for the beam loading.

For the second subharmonic buncher where the bunch width is a δ function compared to 714 MHz, the steady-state beam loading is $\mathrm{Ib} \times (R/Q) \times Qo/(1+\beta)$ =130 kV. The generator power needed to compensate for beam loading plus the bunching voltage is 167.8 kW. The phase shift induced by the steady-state beam loading is $\arctan[135/(34+135)] = 39°$.

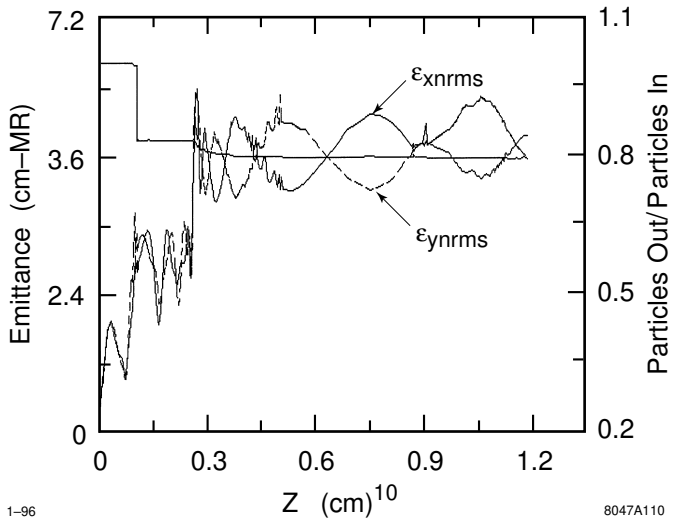

Figure 2-10. *Beam emittance along the injector from gun to the end of the second accelerator section (80 MeV).*

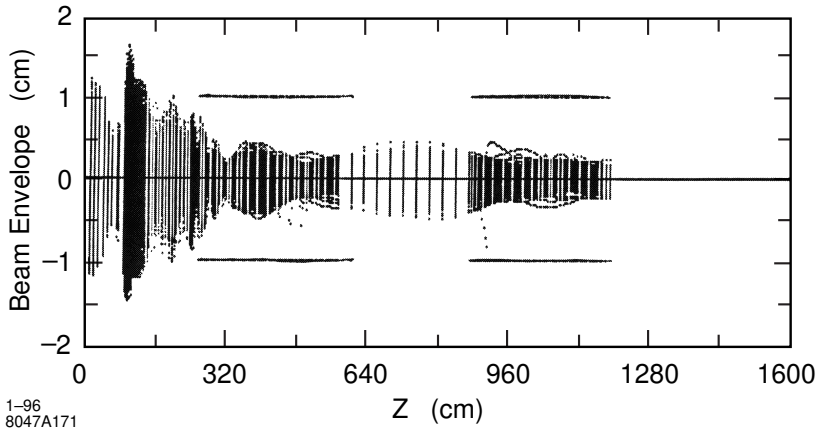

Figure 2-11. *Electron beam edge envelope from gun to end of the second accelerator section (80 MeV).*

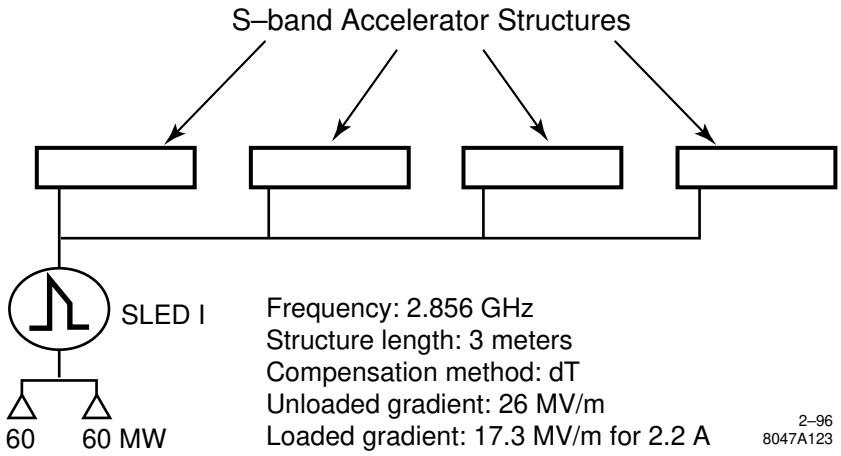

Figure 2-12. *A single module configuration for the 2 GeV electron injector linac.*

2.4.5 Injector Linac

The Linac for accelerating the bunched electrons from 80 MeV to 2 GeV consists of 3-m S-band structures. The nominal rf frequency for the accelerator structures is 2856 MHz. Two SLC model 5045 klystrons drive one SLED1 cavity and the power out of the SLED drives four accelerator sections on one module. Figure 2-12 shows the layout of one module, and the injector for the collision electrons will employ 11 such modules. The beam loading compensation method using the Δt technique for the S-band linac is described in detail in Chapter 6. For the highest charge operating scenario, the maximum current in the injector linac will be 2.2 A. For 2.2 A in the injector linac the maximum possible energy gain per module is 208 MeV with 60-MW usable klystron power. in the accelerating structures. The central energy variation from bunch 1 to bunch 90 is about 0.005% at the end of each accelerator section, and the single bunch energy spread due to the bunch width and assuming the beam is on the crest will be $\pm$0.6% edge.

The lattice from 80 MeV to 2 GeV up to the linac-to-ring transition was designed using MAD. A 30° achromatic bend system at 80 MeV allows us to introduce a second injector line parallel to the first one up to 80 MeV. Two sets of emittance measurement stations are included, one on each side of the bend to measure emittance coming out of the bunching system and the other for measuring the emittance into the 2-GeV accelerator. The transport line from the end of the second accelerating section to the beginning of the first injector linac module has been designed. The lattice is shown in Figure 2-13. The bend is an achromatic and isochronous system consisting of two rectangular dipole magnets which bend the beam by 30°. A FODO lattice with seven identical quads separated by 70 cm from center to center are used. The beam envelope for $\pm$2% energy spread is less than 1 cm in radius at its maximum and comfortably fits in a 1.5-in pipe. The bunch length expansion is only 0.08 ps per 1% energy spread. The total length of the achromatic bend is 4.9 m.

The accelerator lattice is designed to take the $\beta = 1.4$ m beam achieved at the end of the second accelerator with PARMELA simulation and increase it by a factor of the square root of the energy up to 2 GeV. As shown in Figure 2-1, wrap-around quadrupoles are used around the first part of the accelerator section to maintain the small β function at the low energy end where the wakefield effects are more significant. We assumed that each module contributes 192 MeV for the lattice design to allow for some energy overhead.

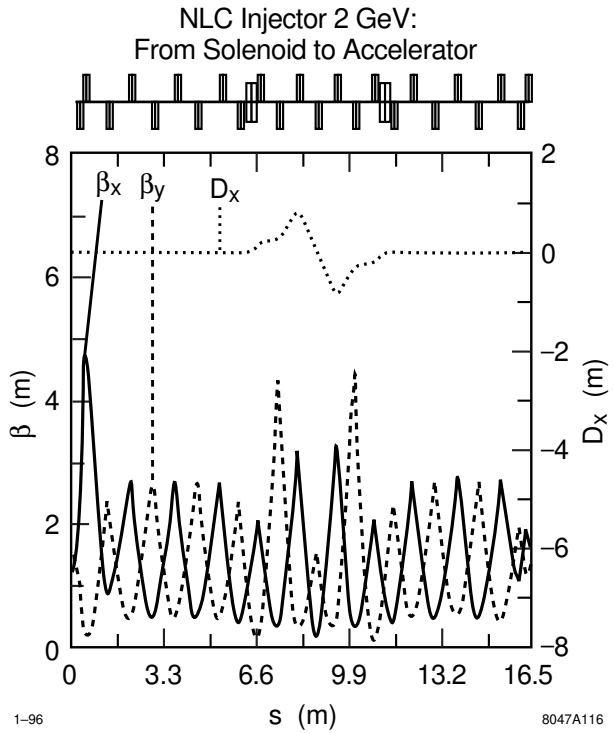

Figure 2-13. *Electron injector lattice to transport beam from the end of the solenoids to the injector accelerator.*

With this assumption, the beam reaches 2 GeV after 10 modules, thus there is an additional module for overhead. While the spare module will not accelerate the beam during normal operation it still needs at least one klystron to be operating for beam loading compensation in that module as described in more detail in Chapter 6. If a klystron fails in one of the accelerating modules then the spare module can be powered in the nominal way while the module with the problem klystron becomes the spare. Figure 2-14 shows the lattice for the accelerator and Figure 2-15 shows the lattice for the matching section from the end of the 2-GeV linac to the linac-to-ring transition. Another emittance measurement station is included in this portion of the injector. Figure 2-16 shows that the pole-tip field of all the quadrupoles in the 2-GeV injector is under 8 kGauss, which is a very comfortable operating range.

The energy spread from the beginning of the train to the end of the train due to beam loading is compensated for completely at the end of each accelerator section. Thus at the doublets between the acceleration sections, the energy spread is uniform from the first to the last bunch and is due only to the single-bunch width. However, at the wrap-around quads on the accelerator sections themselves, at the beginning of the accelerator there is energy variation in the energy of the individual bunches within the train. This is because the gradient at the quad location is different when the first bunch goes by verses when the last bunch goes by. We tracked the first, the middle and the last bunch of the train though the design lattice to see how this effects the emittance out of the injector for the various bunches. We assumed an input single-bunch energy profile which is similar to the energy profile at 80 MeV as calculated by PARMELA, and central energy variation at the wrap-around quads based on the beam loading compensation scheme. Tracking simulations show that at the end of the 2-GeV linac there is only 3% emittance growth in the x plane and none in the y plane. The bends in the 80-MeV achromat are in the x plane.

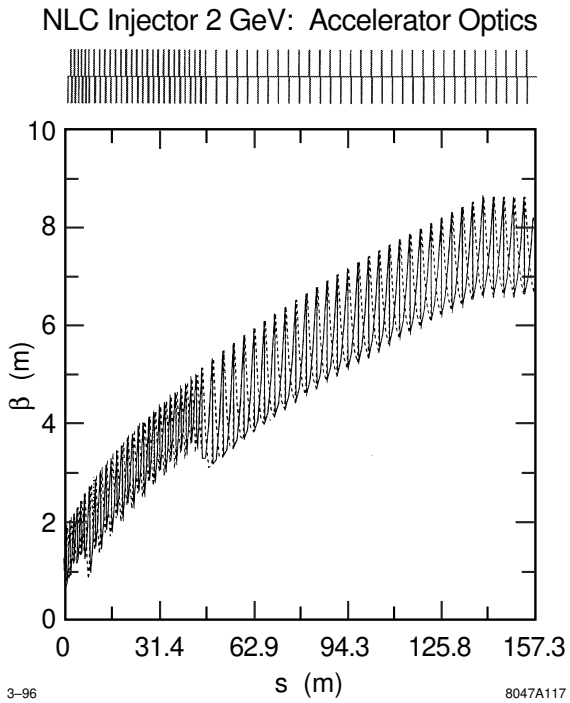

Figure 2-14. *Electron injector lattice over the 2-GeV accelerator.*

The effects of the wakefield on the emittance were estimated assuming that the beam is offset by one sigma from the accelerator centerline and that the β grows as the square root of the energy monotonically starting with 1.5 m at 80 MeV. At 2 GeV the actual emittance of the beam increases by only 4% but the effective emittance growth, taking into account that the beam is not centered, is 44%. Even with this emittance growth the total emittance will be about 0.63×10^{-4} m-rad, well within the 1×10^{-4} m-rad threshold.

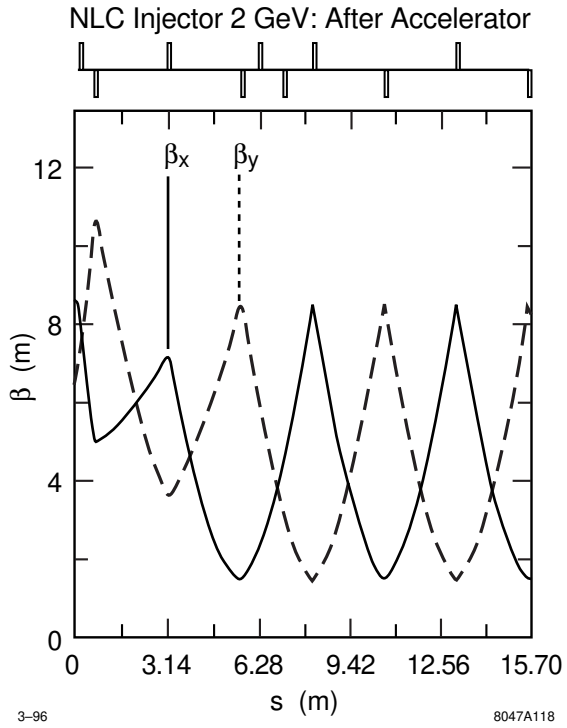

Figure 2-15. *Electron injector lattice from the 2-GeV accelerator up to the damping ring.*

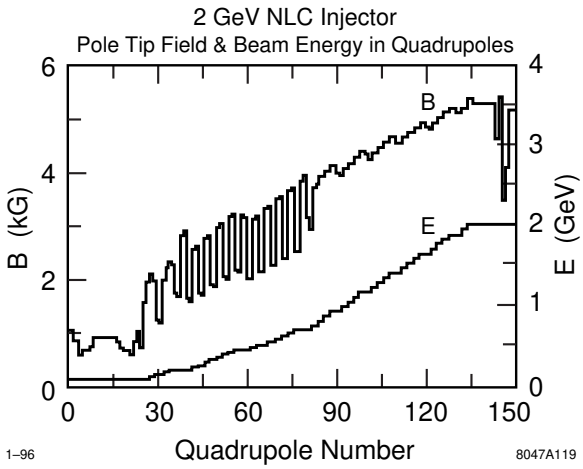

Figure 2-16. *Electron injector quadrupole pole-tip fields and electron beam energy from the end of the solenoids up to the damping ring.*

2.5 Buncher Cavities

There are two types of bunchers: Two standing wave 714-MHz subharmonic bunchers and an S-band traveling wave buncher with four cavities with a phase velocity of 0.75 c. The traveling wave buncher is similar to the one on the SLC and will be integrally brazed onto the first 3-m accelerator structure.

The subharmonic buncher will have the following parameters:

f =	714 MHz
R/Q	$\sim$ 10 W
Q	$\sim$ 10000
β	$\sim$ 1

Subharmonic structures with similar parameters need to be constructed for the NLCTA injector upgrade project, thus much experience is expected to be gained in this area.

2.6 Positron Drive Linac

The linac for the positron drive beam is similar to the injector of the collision electron beam. Two differences are that the positron drive linac will use a thermionic gun and will extend to 3.11 GeV in NLC I and 6.22 GeV in NLC II with optics to transport the electron beam to one of the parallel positron production beam lines. Figure 2-17 shows the electron injector for the positron drive beam. Initially, accelerator sections will be installed to accommodate the 3.11-GeV injector with one module to spare, and room will be left to install accelerating sections to double the energy of the drive beam for NLC II.

The thermionic DC gun rather than a photocathode DC gun is chosen for the positron drive injector because thermionic guns are easier to construct and operate, and they do not have an expensive laser system associated with them. One major difference between the thermionic gun for the NLC and the thermionic gun which was used on the SLC is that the NLC requires a bunch train format right from the gun. The nominal bunch train consists of 90 bunches, each bunch 700 ps in full-width-half-maximum and 1.4-ns apart. In addition, we must be able to change the bunch separation to 2.8 and 5.6 ns. We believe it will be too difficult to achieve all three possible train structures with one pulser, but since the change in train format is not a routine operation and we would be willing to take the time to exchange pulsers, we feel that it would be possible to construct three different pulsers, one for each bunch separation scenario. The 1.4-ns bunch interval pulser can be a resonant pulser while the other two would have to be broad-band pulsers similar to the ones constructed for the KEK Advanced Test Facility thermionic gun [Naito 1994].

The positron drive injector beamline from the gun through 80 MeV is identical to the polarized e-beam injector. The lattice from 80 MeV to the spoiler in front of the positron target in either of the two parallel positron production lines has been designed. Figure 2-18 shows the β function from 80 MeV though the 3.11-GeV linac and the allocated space for additional accelerators for NLC II. Figure 2-19 shows the β function for the beam transport from the end of the accelerator to the spoiler including the 10° achromatic bend to switch the beam to either of the positron production lines. The beam size at the spoiler in front of the positron target is designed to be $\sigma = 0.5$ mm, about 1/3 of the size required at the target after the spoiler. Figure 2-20 shows the quadrupole pole-tip strengths for the positron drive beam linac which are at very reasonable values at less than 8 kGauss.

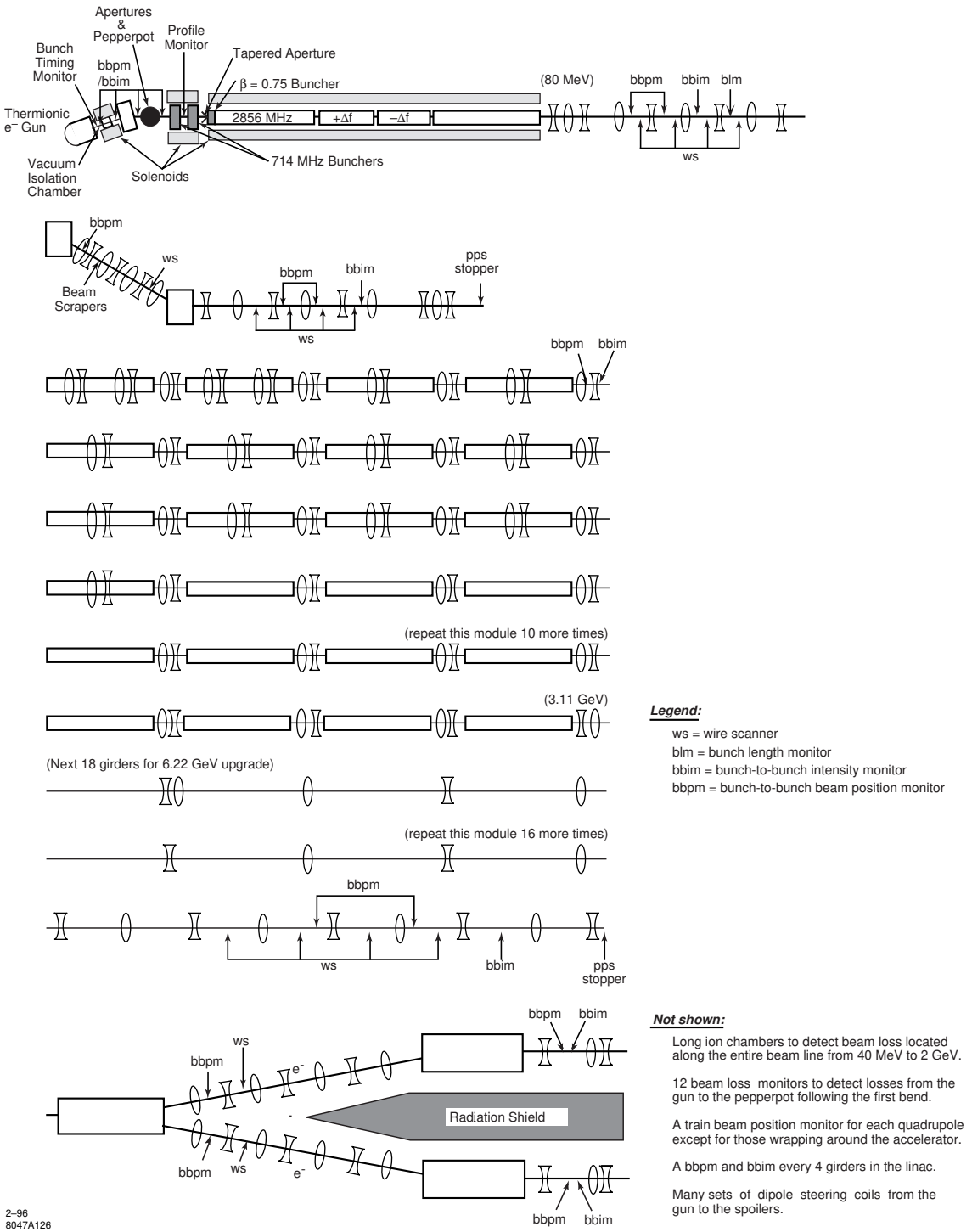

Figure 2-17. *Electron linac for the positron drive beam.*

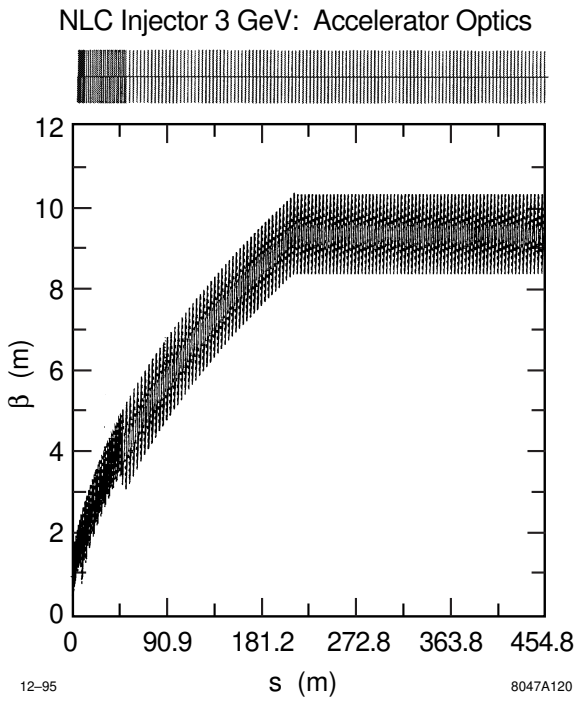

Figure 2-18. *Positron drive linac lattice to transport the electron beam from the end of the solenoids to the bend at the end of the drive linac.*

As mentioned before, the β function and the beam line up to 2 GeV is identical to the collision electron case but the β continues to grow as the square root of the energy up to 3.11 GeV in this lattice. Using these parameters, the wakefield contribution to emittance growth was estimated for the 3.11-GeV linac in a similar way as for the 2-GeV collisions electron injector linac. The actual beam emittance of the last bunch increases by 11% at the end of the 3.11-GeV linac but the effective emittance increase due to the beam being offset by one sigma is 52%. This is still acceptable for the drive injector for positron production.

No special difficulties are expected with the positron drive injector which have not already been taken into consideration for the collision electrons.

2.7 Diagnostics

The purpose of the diagnostics system is several-fold: to aid in tuning the injector, to diagnose the beam parameters including jitter, and to be used for machine protection triggers. The diagnostics consist of charge monitors and beam position monitors some of which are capable of measuring the parameters for a small group of bunches in a portion of the train selected by the user, bunch-to-bunch timing monitor, aperture/pepperpot insert, beam profile monitors, bunch length monitor, emittance measurement and energy spread measurement stations after 80 MeV and 2 GeV. There is a rather high density of current monitors and position monitors in the beam line from the gun through 80 MeV. Every doublet in the injector linac has a beam position monitor in it. There will be microchannel-plate photomultiplier-tube beam loss monitors in the 120-keV region and a PLIC cable in the region from 40 MeV and beyond.

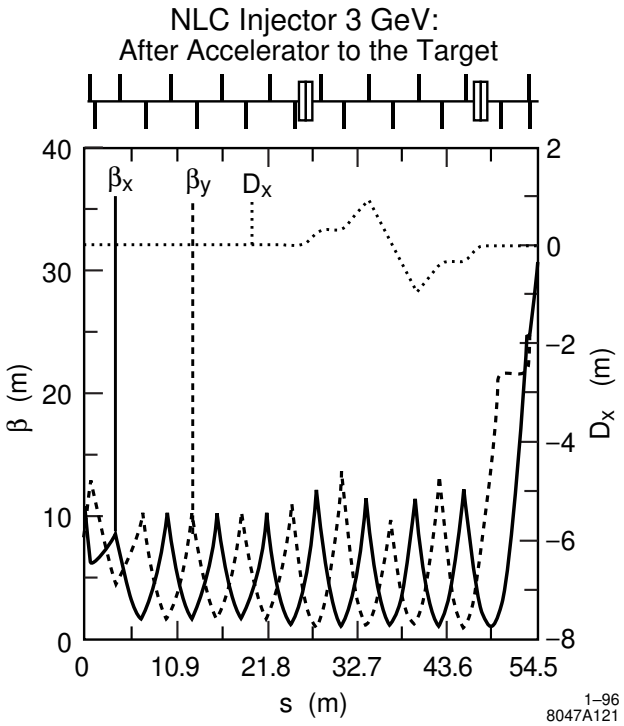

Figure 2-19. *Positron drive beam lattice from the end of the diagnostics station after the drive linac up to the spoiler.*

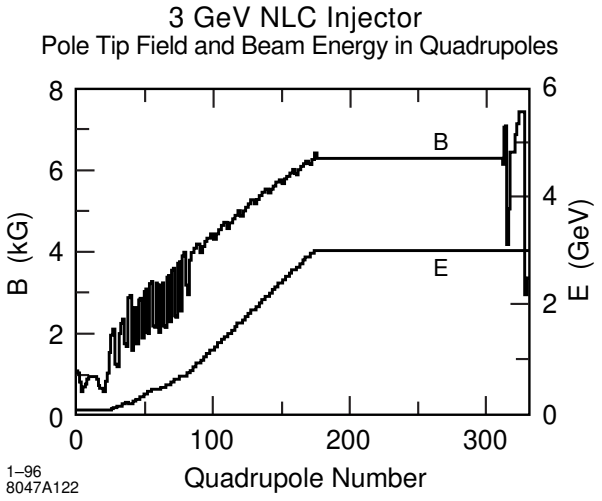

Figure 2-20. *3-GeV NLC injector. Pole-tip field and beam energy in quadrupoles.*

Diagnostic	Total Bunch Train		Bunch bundle[a]	
	Range	Resolution	Range per bunch	Resolution per bunch
Toroid charge mon.	45–250 $\times 10^{10}$ e^-	±0.2%	0.5–3 $\times 10^{10}$ e^-	±1%
Gap current mon.				
charge	45–250 $\times 10^{10}$ e^-	±3%	0.5–3 $\times 10^{10}$ e^-	±3%
pulse width	1–150 ns	±1 ns	∼200 ps	—
Streak Camera	1–150 ns	±1 ns	5–40 ps	1 ps
Beam loss mon.	0–10^8 e^-	10^7 e^-	—	—
Beam position mon.	0–1 cm	±20μ	0–1 cm	±20μ
Beam size mon.				
at the cathode[b]	R=0 - 1.5 cm edge	±1%	R=0 - 1.5 cm edge	±1%
at 120 keV	R=0 - 1.5 cm edge	±1%	R=0 - 1.5 cm edge	±1%
at 80 MeV	R=0.2 - 1 cm edge	±1%	R=0.2 - 1 cm edge	±1%
Energy	80 MeV	±0.2%	∼80 MeV	±0.5%
Energy spread at 80 MeV	∼4%	±0.2%	∼4%	±0.2%
Pepper pot	Qualitative diagnostic			
Bunch length monitor	Qualitative measurement for tuning by maximizing signal			

[a] Bunch bundle represents a group of bunches as close to a single bunch as possible. Some of the diagnostics may not be fast or sensitive enough to measure single bunch parameters but can measure a group of about five adjacent bunches and this would be sufficient. These diagnostics would require a timing gate width of about 3 ns, with a 0.5-ns rise time and 10-ps timing stability. The details of how to construct such diagnostics will be covered in Chapter 15.

[b] A profile of the laser at a screen located at the image point of the cathode.

Table 2-3. *Injector diagnostics and their specifications.*

Most of the monitors at the gun and at the end of the first accelerator section need to have the ability to measure variation from bunch-to-bunch within the same bunch train. Measuring the variation between a group of bunches in 5-ns intervals would be sufficient, that is, it is not necessary to measure the parameter of a single bunch.

Figure 2-1 shows the various kinds of monitors on the e^- injector beam line. The drive linac for the positrons will have these same diagnostics except the wire scanners for the linac emittance measurement will be located just upstream of the achromatic bends up to the two positron production lines. In addition there will be bunch-to-bunch beam position monitors, intensity monitors and wire scanners in the achromatic bends and just upstream of the spoilers as shown in Figure 2-17.

Table 2-3 shows the various diagnostics in the injector, and their specifications.

2.8 Operation

2.8.1 Initial Set-up and Beam Maintenance

Figure 2-1 shows a schematic of the injector beam line components from the gun anode up to 2 GeV. Each of the subharmonic bunchers, the S-band buncher and the S-band accelerator sections will have independent rf phase and amplitude control. There are beam steering coils at the gun and after the bend. Large steering coils are draped over the solenoids from the subharmonic bunchers through the second accelerator section. There is a set of steering coils on each module in the injector linac.

The procedure for operating the NLC injector has several aspects. First of all it is necessary to set the focusing, bunching, and accelerating parameters of the injector to the optimum values for beam transport and quality. Then it is necessary to maintain the optimized beam quality achieved during startup over a long period of time. Finally it is necessary to establish guidelines for troubleshooting problems when the beam quality deteriorates. Additionally, it is necessary to establish good, clean configuration records to aid in recovering from various faults or down times.

To set up the injector parameters initially, it is necessary first of all to have good calibration data on all the beam diagnostics, the various power supplies, and rf drivers including the losses in cables and processing electronics. It is necessary to characterize the subharmonic bunchers and buncher and accelerating sections so that one can actually convert the power measured at the test points into electric fields as the beam sees it. Having calibrated the various components such that one can determine the state of the injector and the beam in it, we can then start the tuning procedure.

At first and when turning on the beam after long down times, it is necessary to establish a good quality, single-bunch beam all the way to the end of the injector before going to long-pulse operation.

The first order of business is to establish beam from the gun by shaping and pointing the laser on the photocathode and adjusting its power for the desired charge from the gun. Next, the beam is transported around the 20° bend to the subharmonic buncher by using the magnetic lens and solenoid strengths designated by the simulations and by steering. Once the beam reaches the subharmonic bunchers, it is necessary to synchronize the beam with the rf of the Subharmonic bunchers, the accelerators, the current monitor, and beam position monitor sampling cycles. Next, we need to bunch the beam and steer it to achieve at least 80% of the gun charge captured in 18 ps at 80 MeV. It might also be necessary to adjust the strengths of the axial magnetic field coils to achieve the simulation beam size at the profile monitor. Next, we steer the beam in the injector linac while phasing the klystrons to maximize the energy using the energy spread wire scanners both in the chicane at 80 MeV and 2 GeV. Once the desired quality beam is achieved at the end of the injector, all configurations and beam parameters should be archived for future use.

Now it is time to lengthen the train gradually without losing beam on the monitors all the way to the end of the injector. The subharmonic buncher timing and the phase of the compensating klystrons is adjusted slowly to maximize the signal on the bunch length monitor and to minimize the energy spread on the energy spread wire scanners. Once the long bunch train configuration is set, we can then adjust the intensity jitter limiting aperture for the optimal size. This process also has to be done slowly, adjusting the timing of the subharmonic buncher and the power in the compensating klystrons at the same time. Next we can use the scrapers in the 80-MeV chicane to clip away the tails. More adjustment of the power in the compensating klystrons will be necessary.

Configuration files showing the orbit and charge transmission of the beam throughout the injector and all the device settings will be saved. In addition, the bunch length, the energy and energy spread, the emittance of the beam at 80 MeV, and at the entrance to the damping ring should be measured. This information is important for expediting the accelerator setup in the future and maintaining the beam quality in a consistent way.

To maintain the beam quality day-to-day, various steering and energy feedback systems will be used. RF and magnet parameters, as well as beam parameters, will be compared to the parameters in the best saved configuration files and flagged if they are off by more than the allowed tolerance.

2.8.2 Troubleshooting

Some of the typical things that can go wrong in the injector are that the energy spread of the beam downstream, for example, at the damping ring is too large. If this spread cannot be reduced to an acceptable size by phasing the accelerators, most likely the phases of the bunching components have drifted away from optimum. Check their phase and amplitude against the saved optimized configuration and make the necessary changes. It is important to simultaneously maximize the signal at the bunch length monitor

Another problem could be the increase in energy jitter. This usually stems from rf-amplitude jitter in the accelerator or bunching rf sources and should be fixed by the rf technicians.

Another problem could be the increase in intensity jitter. This could stem from a number of reasons. Check the intensity jitter of the laser as it will be running on the edge of available technology as far as intensity jitter is concerned. Another cause for intensity jitter is when the beam is large compared to the various apertures and is not centered, thus is being scraped. One can check this with the various screens and PLIC signals. The most effective knobs for solving this problem are the small lenses near the gun and after the bend and the second most effective are the steering coils.

It is impossible to enumerate all the possible problems which can occur in the injector area, but we have addressed the most common ones.

2.9 Conclusion

The NLC polarized source injector will be a conventional injector employing subharmonic bunching to achieve the required bunch intensity and structure. Simulation results show that it is possible to capture 83% of the charge into the subharmonic buncher system into 18-ps bunches when a train of bunches are produced from the gun which are 700-ps wide and 1.4-ns apart. The total energy spread at 2 GeV is expected to be $\pm 0.6\%$, well under the $\pm 1\%$ threshold. The emittance, including wakefield effects, is expected to be less than 0.6×10^{-4} m-rad, well within the about 1×10^{-4} m-rad threshold. The charge intensity jitter limiting aperture is able to reduce 2% incoming intensity jitter to an immeasurable amount at the cost of losing 17% of the charge from the gun. Using the Δt compensation technique in the injector linac, we can reduce the bunch train energy spread without any effect on the single-bunch energy spread at the end of the injector.

The injectors for both the collision and positron drive electron beams are almost identical up to 2 GeV with the exception that the positron drive injector will use a thermionic gun. This should allow us to reduce construction costs and operational complications.

The NLC injector scheme is similar to the current SLC injector with the added complication of working with a long bunch train instead of a single bunch. There are several issues regarding this added complication which deserve a hard look either in detailed simulations and or demonstrations in a laboratory environment. The R&D programs needed to ensure us of success with the NLC injector are: 1) The cathode charge limit as addressed in Appendix 2.B. 2) The beam-loading compensation in the bunching system. 3) Demonstrate the production of the 1.4-ns-separation bunch train in the thermionic gun. 4) Development of a reliable and stable polarized source rf gun to produce small emittance beams from the injector, thus simplifying the operation and maybe the design of the damping ring. Item 1) can be studied in the SLC polarized source laboratory. Item 2) and 3) will be demonstrated in the NLCTA upgrade. There are several options for demonstrating item 4). One of these options would be to use the rf gun test stand being constructed at SSRL.

Despite the differences between the SLC and NLC sources, experience with the SLC can be applied and extended for a reliable and stable operation of the NLC injector.

2.A Polarized e^- Beam Photocathode RF Gun Development for the NLC

2.A.1 Introduction

While the baseline injector design for the NLC polarized electron source is presently a conventional polarized DC gun with a subharmonic bunching system, the development of a low-emittance polarized electron beam rf gun in parallel, as a possible future upgrade, is important to simplify the damping ring design and/or operation.

Polarized e^- beam photocathode rf gun injectors are an attractive alternative to the conventional electron source for the NLC because of the possibility of achieving very low electron beam transverse emittance and thus making it possible to reduce the size of the damping ring or at least making it easier to operate. Simulation results show that it is possible to achieve normalized rms emittance of $\epsilon_{n,\mathrm{rms}} = 1$ mm-mr for a 1 nC bunch, 10 to 20 ps in width [Gallardo 1993, Palmer 1995b, Sheffield 1993]. Some experiments have been conducted at LANL and BNL to achieve beams which are very similar in quality to these simulation results. The low emittances are achieved due in part to the emittance compensation technique discussed in reference [Carlsten 1989]. The NLC requirements for the beam from the rf gun are about 4 nC in a 10 to 20-ps bunch 1.4-ns apart in a train of 126 ns. The normalized, rms emittance requirements at the input of the current NLC damping ring design is $< 10^{-4}$ mm-mr rms at the damping ring. The emittance damping time in the ring depends on the emittance of the incoming beam. For each order of magnitude reduction in the input beam emittance, the number of bunch trains to be simultaneously stored in the ring can be reduced by 1, thus also reducing the size of the ring. Even a factor of 2 or 3 reduction in emittance would be helpful in improving the operation of the damping ring even if its design is not simplified.

Photocathode rf guns have shown themselves to be a stable and reliable source for the FEL community [Travier 1994]. In the NLC, Cylindrically Symmetric Emittance-Compensated Polarized RF Gun Development program, the work of the FEL community would be extended to the development of a polarized source, emittance-compensated, ultra-high-vacuum rf gun. This new gun design would address the issues associated with polarized rf guns some of which are discussed in reference [Clendenin]. The main technical issues to resolve for polarized rf guns which are more difficult than for the DC guns are: 1) A stable and reliable pulsed laser system to produce the electron bunch train, 2) the beam dynamics associated with producing a

low-emittance electron bunch train including the possible depolarization effects due to strong space charge and transverse magnetic fields near the cathode, 3) elimination of field asymmetries in the gun which will cause emittance growth, 4) the ultra-high-vacuum environment which is difficult to achieve in rf guns but is required by the GaAs cathodes for long lifetimes, 5) the effect of high-gradient fields on GaAs cathodes, 6) cathode issues such as promptness of the photoemission, cathode lifetimes and quantum efficiency, and 7) finally, the reliable and efficient operation as a injector system.

A development program for an asymmetric beam rf gun is also important, since the emittance required at the interaction point is two orders of magnitude smaller in the vertical plane than in the horizontal plane. An asymmetric beam could be produced at the cathode of the rf gun by the production of an asymmetric transverse laser pulse. This program would initially proceed with the unpolarized source, emittance-compensated rf gun, since the flat-beam emittance compensation has not yet been experimentally demonstrated.

2.A.2 Beam Dynamics

In this section we shall discuss two parallel R&D efforts that will elucidate two areas of accelerator physics and in the end allow the combining of these developments to produce a flat-beam polarized rf gun.

The study of negative electron affinity (NEA) GaAs in high-gradient fields, along with the development of a dedicated cylindrically symmetric, polarized-source rf gun facility is one of these development programs.

Intensive programs to study and demonstrate low-emittance, high-brightness beams from symmetric photocathode rf guns is ongoing at LANL, BNL, SLAC, UCLA and other laboratories abroad. The best available symmetric rf gun emerging from these studies should be used for studying the survivability of polarized e^- source cathodes in rf guns. This will allow for the study of vacuum conditions, field amplitudes, and cesiation processes that are necessary for the production of polarized electrons without the additional problems of flat-beam production.

In another development program for the flat electron beam production, the physics of emittance compensation of a flat-beam and rf field uniformity can be addressed without the added difficulty of polarized electron production.

Round Beam

PARMELA simulations of injectors for FELs show that it is possible to produce an electron beam with a transverse normalized emittance of $\epsilon_{n,\mathrm{rms}} = 1$ mm-mr. The beam parameters from these simulations are listed in Table 2-4 and shown in Figure 2-21. Simulation studies of L- and C- band systems are ongoing using the S-band system as a baseline [Kirk 1995].

The emittance compensation scheme realigns different "slices" [Sheffield 1992] of an electron bunch. Depending on the cathode spot size, total charge per bunch, and peak field at the cathode, the precise position of the compensation solenoid [Palmer 1995a] is critical. Figure 2-22 shows this for the parameter set in Table 2-4. In the physical construction of the gun and solenoid magnet, the waveguide physically limits the position of the magnet with respect to the cathode of the gun. This problem has been corrected in the proposed L-band rf gun being designed for the TESLA X-ray FEL [TESLA FEL]. It uses a "door-knob" rf coupler downstream of the full cell, eliminating the physical constraint of the waveguide and maintaining cylindrical symmetry. As a result, this scheme eliminates the higher-order spatial harmonics that can also

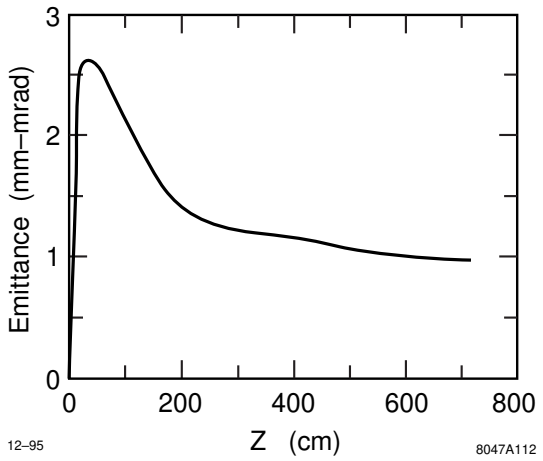

Figure 2-21. *PARMELA simulations of emittance compensation for the BNL/SLAC/UCLA S-band rf gun*

Total Charge	1 nC
Number of particles	10K
Cathode Spot Size	1 mm radius
Longitudinal Profile	Flat-top
Transverse Profile	Flat-top
Initial Cathode KE	.5 eV
Initial Thermal Emittance, ϵ_o	0 mm-mr
$E_{\,Full\ Cell}/E_{\,Half\ Cell}$	1.00
E_o *at Cathode*	160 MV/m

Table 2-4. *Electron bunch parameters used in PARMELA.*

cause emittance growth, and allows for the precise positioning of the compensation magnet. The tuners and vacuum connections to the gun will also physically limit the magnet position, but these problems can be eliminated by longitudinal connections to the gun body versus radial coupling used in the previous gun designs.

Asymmetric Emittance RF Photocathode Electron Sources for the NLC

While the expected performance of cylindrically symmetric rf gun photo-injector systems is well understood from theoretical analysis and simulation, which have been benchmarked by experiment, an extension to a fully three-dimensional approach has not until recently been undertaken by investigators at UCLA and Fermilab. This effort has been motivated by the demands of the superconducting TESLA linear collider design, in which the normalized emittances are $\epsilon_{x,y}$=20, 1 mm-mr at Q=8.3 nC. In this machine, it is possible to have asymmetric emittances at the injection point of an electron linac which meet the constraints set by the interaction point. While the emittances may not be low enough to eliminate the need for an

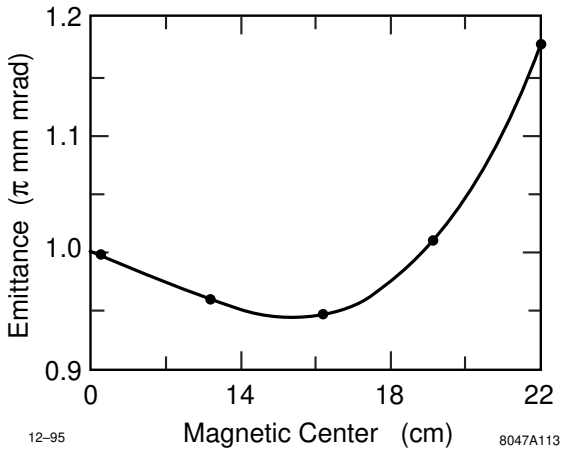

Figure 2-22. *Optimized emittance versus magnetic center.*

electron damping ring in the NLC designs under consideration here, benefits in designing and operating the damping ring may be derived from injection of lower, asymmetric-emittance electron beams.

To state simply, the approach to design an asymmetric rf photoinjector source [Rosenzweig 1993], one uses the fact that the temperature of the emitted beam particles from a photocathode is only a function of cathode material and laser photon energy. This allows the creation of asymmetric emittances $\epsilon_x \gg \epsilon_y$ by illuminating the photocathode with a ribbon laser pulse ($\sigma_x \gg \sigma_y$). Typically, the dominant emittance growth mechanism at relevant current densities is space-charge, and this is conveniently mitigated by the ribbon geometry of the electron beam pulse. One must also pay attention to the potential for rf-induced emittance growth, especially in the horizontal dimension where the beam is large. In the spirit of the problem for cylindrically symmetric systems performed by K.J. Kim [Kim 1989], we have examined the scaling of emittances with respect to beam dimensions, accelerating gradient and phase, and beam charge. The "thermal" contribution to the emittance given by the finite spread in transverse momenta of photo-emitted electrons is, assuming 0.1 eV emission temperature (typical of semiconductors),

$$\epsilon_{x,y}^{th} \cong \sqrt{\frac{kT_\perp}{m_e c^2}}\sigma_{x,y} \cong 0.25\sigma_{x,y}\,(\mathbf{mm})\ \text{mm-mr} \tag{2.4}$$

For TESLA, this implies beam sizes of $\sigma_x < 4\,\text{cm}$, and $\sigma_y < 2\,\text{mm}$, while for the NLC requirements we must have $\sigma_x < 0.4\,\text{cm}$, and $\sigma_y < 0.2\,\text{mm}$. This is a potential challenge for the NLC cases, because a $Q = 4\,\text{nC}$ beam of such a small cross-section implies an accelerating field needed at the cathode to overcome longitudinal space charge of E>72 MV/ m at injection. Under the assumptions of a cylindrically symmetric rf cavity structure, it is easy to derive the minimum rf contribution to the rms emittances, which can be written as

$$\epsilon_{x,y}^{rf} \cong \frac{eE_{rf}}{\sqrt{8}m_e c^2}\sigma_{x,y}^2\,(\Delta\phi)^2 \tag{2.5}$$

where $\Delta\phi = \left(\frac{\omega}{c}\right)\sigma_z$ is the phase extent of the beam. Minimizing these quantities implies operation at low frequency, low accelerating gradient, and with small bunch sizes in all dimensions. For our case, we are considering a fairly large horizontal beam size as well as high gradient, and so this is an issue for the horizontal emittance.

There are a number of proposed ways to remove or minimize the emittance-diluting phase-dependent defocusing due to the transverse rf forces in the gun. Because of the use of emittance compensation to deal

with the space-charge contribution to the emittance, it is perhaps wisest to use a scheme which mitigates the transverse kick in the x direction. This can be accomplished by removing as best as possible the dependence of the rf fields on x. It should be noted in this regard that the defocusing kick induced at the end of a cylindrically symmetric cavity is approximately equal parts electric and magnetic. The electric component of the kick is mainly due to the fringing fields near the iris at the exit of the gun. The fringe field can be made mainly vertical simply by making the iris opening a slit, long in the horizontal dimension.

The magnetic component, however, cannot be so easily diminished, as it is not dependent on the iris, but on the accelerating field in the interior of the cavity. The only way to diminish the magnetic force in the horizontal direction is to break the symmetry of the cavity outer wall. The simplest asymmetric structure is a rectangular box cavity, but this only diminishes (does not eliminate) the horizontal rf forces, and produces a sinusoidal dependence of the accelerating field on the x dimension. A better choice is to use an "H-shaped" structure (as suggested by R. Miller), which has been investigated in the context of sheet-beam klystron development at SLAC. In this structure, the accelerating field in the "bar" region of the H-cavity has no dependence on x and therefore has acceleration independent of transverse position, as in a symmetric structure. It should be noted that the vertical forces (which are due mainly to the backward speed-of-light space harmonic in this p-mode structure), in this case in the bar region, are now entirely in the vertical dimension, and are twice as large as the equivalent symmetric cavity. The function of the side regions is to allow the longitudinal field to go to zero sinusoidally, to satisfy the boundary condition, and choose (along with the vertical dimension) the cavity resonant frequency.

An analysis of the space-charge contribution to the emittance gives the following scaling, derived from both approximate analysis and PARMELA simulation [Rosenzweig 1995]:

$$\epsilon_{x,y}^{sc} \approx \frac{2N_b r_e}{7\sigma_{x,y}W} e^{-3\sqrt{W\sigma_y}} \sqrt{\frac{\sigma_y}{\sigma_z}} \tag{2.6}$$

$$W = \frac{eE_{rf}}{2m_e c^2} \sin(\phi_o) \tag{2.7}$$

Here, $\epsilon_x^{sc} \approx \frac{\sigma_x}{\sigma_y}\epsilon_y^{sc}$ is approximately obeyed; this is a consequence of the fact that for an ellipsoidal charge distribution, the normal electric field at any bunch boundary is approximately the same as any other. It should be noted that minimizing the space-charge contributions to the emittances implies operation at high accelerating gradient. It should also be emphasized at this point that these emittances, induced by the space charge at low energy, are mainly due to the different orientations of each "z-slice" of the beam. A scheme is discussed below, emittance compensation, which can remove these correlations, effectively lowering the emittances of the bunch. Before taking up this discussion, it should also be pointed out that one cannot arbitrarily reduce σ_y, because of the limit on surface charge density emitted from the cathode before the retarding space-charge cuts off emission ($\sigma_x\sigma_y > 2\frac{Q}{E_z}$).

This effect has been observed at UCLA. It is instructive to look at the product of the emittances, to see if there is some chance of achieving the desired emittances without the need the for emittance compensation

$$\epsilon_x^{sc}\epsilon_y^{sc} \approx \left[\frac{2N_b r_e}{7W}\right]^2 \frac{e^{-6\sqrt{W\sigma_y}}}{\sigma_x \sigma z} \tag{2.8}$$

The argument in the exponential in this expression is generally smaller than one for reasonable accelerating gradients, and so one can see that, in general, a beam large in the longitudinal and horizontal dimensions is needed to minimize the product of the space- charge emittances. Unfortunately, these are precisely the dimensions that the rf contributions are sensitive to, and thus one cannot consider making them arbitrarily large. As an example of a design where the rf contribution is not yet significant, we take $N_b = 5*10^{10}$, W=80,

$\sigma_z = 2\,\mathrm{mm}$, $\sigma_x = 2\,\mathrm{cm}$, $\sigma_y = 1\,\mathrm{mm}$. In this case, we have $\epsilon_x^{sc}\epsilon_y^{sc} \approx 450$, as opposed to $\epsilon_x^{sc}\epsilon_y^{sc} \approx 20 \sim 50$ as needed by TESLA, and we miss the design goal by an minimum of three to four in both dimensions. For the NLC case, the degree to which the design goals will not be met without emittance correction is even larger.

It is apparent that further efforts must be made to achieve the emittances needed for linear collider designs; that is, one must employ an emittance compensation scheme for sheet beams accelerated in asymmetric rf structures. Emittance compensation is essentially a process by which the correlations (mainly as a function of the longitudinal position in the bunch) in the beam's transverse phase space that are induced by space-charge forces operating at low energy (in the photocathode gun), are removed by focusing the beam, reversing the direction of additional correlations. When the orientation of the transverse phase space ellipse of each "z-slice" has the same angle, the linear component of the emittance due to this effect is removed. Since the space-charge forces must still be large enough after the focusing lens to allow for compensation, this scheme tends to work better at lower accelerating gradients for convenient focusing geometries. This happy direction in the design of the system allows us to mitigate concerns about the rf contribution to the emittance, and about peak and average rf power (source and heat dissipation problems), in both the symmetric and asymmetric cases. In the asymmetric case, we must have the rf contribution to the transverse phase space trajectories be small, or else the space-charge compensation will suffer from interference. This condition is achieved by the choice of large aspect ratio (sheet) beam profile, and the asymmetric structure described above.

While the serious design calculations must be performed with simulation programs which include as many real experimental effects as possible, these are very time consuming. One needs to have a model with which to predict the approximate behavior of the system before proceeding to simulation. This has been developed; it is a program which integrates the envelope equations for a number of different "z-slices," at positions. The focusing can arise from conventional quadrupole focusing, or from the first order transient kicks It is apparent that further efforts must be experienced by electrons at the exit and the entrance of the rf cavities, and the second order (alternating gradient focusing) in the interior of the rf cavities. Solenoidal focusing is not allowed in this device, because of a coupling of the x and y phase planes due to an $\vec{E} \times \vec{B}$ rotation which is, of course, dependent on longitudinal position in the beam. The emittance terms included in the envelope calculations are only the thermal components.

The results of a typical calculation are shown in Figure 2-23. In this case, the vertical emittance is well compensated, while there is essentially no improvement in the horizontal emittance. This is because the effective defocusing strength associated with the space charge is different in the two dimensions, as can be seen from the envelope equation

$$K_{x,y}^{sc} = \frac{4I\,(z_i)}{I_o\gamma^3\,(\sigma_x + \sigma_y)\,\sigma_{x,y}} \quad . \tag{2.9}$$

Because of this, the compensation process generally proceeds much faster in the small dimension, and thus it is difficult to design a system which simultaneously compensates in the vertical and horizontal dimensions.

The solution to this difficulty is straightforward: since the beam near the cathode is very much larger in x than in y or z, one can effectively remove the dynamics in the x direction (and the dependence on x of the y and z components of the space-charge forces), as is already done for the rf contributions, from consideration by making the beam distribution uniform in x. The effect of this is illuminated by Figure 2-24, which displays the x component of the force along the x axis of the bunch, and the y component of the force at one sigma in y, in the y-z plane, for two cases: (a) where the beam distribution is Gaussian in all three dimensions, and (b) where it is Gaussian in y and z, but uniform up to a hard boundary in x. It can be seen that for the tri-Gaussian beam that the horizontal forces rise approximately linearly to a large value at about one sigma in x. For the uniform distribution in x, however, there is very little horizontal field over about 85 to 90% of the beam, and the field rises steeply and nonlinearly near the beam boundary. As was noted before, the

maximum field is nearly the same, but the region of the beam which is affected is much smaller. Note that the vertical field is also nearly uniform over almost all of the beam, again degrading near the beam edge. In practice, one uses this final 10 to 15% of the beam as "guard charge" during the compensation to remove the horizontal field and homogenize the vertical field, then removes it by collimation after the linac section. In this way, one effectively removes the x dimension from the compensation problem, reducing the problem to two dimensions, as in the (by now well understood) cylindrically symmetric case. It should be noted in this regard that the multiple-envelope model for emittance compensation dynamics has been compared extensively to simulation as well as extended analytically by Serafini and Rosenzwieg [Serafini 1995], and essentially validated for cylindrically symmetric beams. Benchmarking of the models in the asymmetric case awaits further refinements of three-dimensional computational tools.

The expected emittances in the case of a 2856-MHz, 1.5 or 4-nC can be scaled from the previously investigated 1300-MHz, 10-nC, 35-MV/ m rf gun TESLA case, where the emittances are $\epsilon_{x,y} = 30, 2$ mm-mr. The beam dimensions, charge, electromagnetic fields, and emittances all scale linearly with rf wavelength, while scaling of charge at a given wavelength scales the emittances approximately linearly with the charge. Thus we expect that a 77-MV/ m rf gun at 2856 MHz should produce emittances of approximately $\epsilon_{x,y} = 4.5, 0.3$ mm-mr at 1.5 nC and $\epsilon_{x,y} = 12, 0.8$ mm-mr at 4 nC.

2.A.3 Material and RF Considerations

Vacuum

It has been the SLC polarized-source experience that for successful and reliable operation, the vacuum in the vicinity of the cathode needs to be extremely low, on the order of 10^{-11} Torr and the partial pressure of some diatomic gases such as CO must be maintained in the mid 10^{-12} range [Schultz 1992]. The ultra-high-vacuum system is a critical part of making the polarized-electron rf gun work, not only because of the cathode but also to prevent any possible rf arcing in the gun, thus damaging the cathode. Some great progress has been made in Japan in selecting appropriate copper and treating it with pressurized ultrapure water to achieve vacuum levels of 2×10^{-10} Torr in an S-band standing-wave cavity. The cavity was excited with a 2856-MHz klystron, and surface gradients of 337 MV/m were achieved without arcing or any rise in the pressure in the presence of rf [Yoshioka 1994, Matsumoto 1994]. Demonstration of the survivability of the polarized cathode in the rf gun is needed.

It has been proposed that the new 1.6-cell rf gun designed by the BNL/SLAC/UCLA collaboration be constructed out of High Isostatic Pressure(HIP) processed Oxygen Free High Conductive (OFHC) Cu [Palmer priv] to minimize the vacuum problems associated with a high-gradient gun. This gun has been symmetrized to remove the dipole-like spatial harmonic of E_z. It has been proposed that future guns of the BNL/SLAC/UCLA collaboration have their quadrapole-type fields symmetrized thereby eliminating the next higher-order mode emittance growth factor. This would allow for more pumping on the gun and thereby reduce the ultimate vacuum limit.

Assuming that the out-gassing rate of copper is 10^{-12} Torr $\ell/\,\mathrm{s\,cm^2}$, an estimate of the needed pumping speed can be calculated. The total surface area of a state-of-the-art, BNL-type, S-band rf gun is on the order of 420 $\mathrm{cm^2}$. Therefore this type of rf gun will need 42 $\ell/\,\mathrm{s}$ of total pumping speed to maintain the gun vacuum on the order of 10^{-11} Torr. This amount of pumping does not take into account the conductance-limiting effects of the waveguide to full-cell coupling iris.

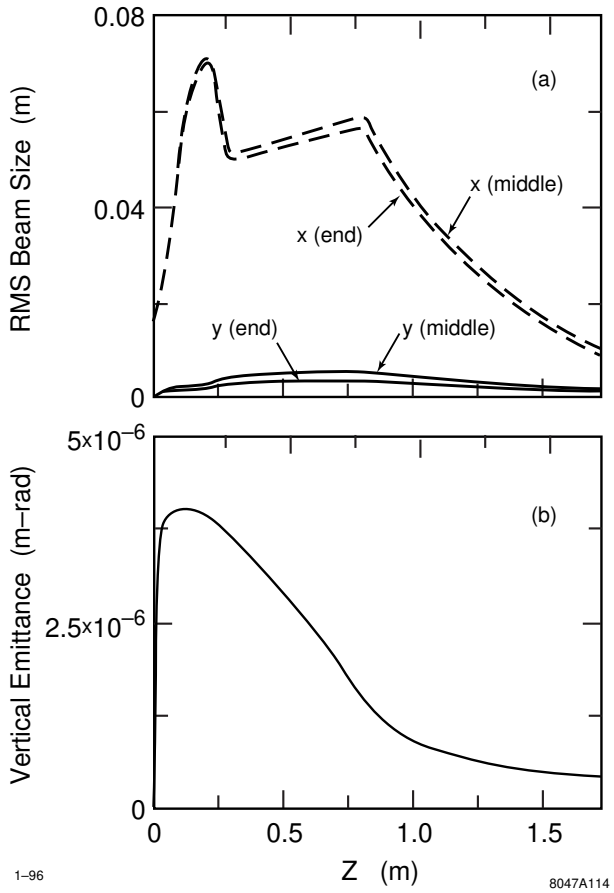

Figure 2-23. *(a) Rms beam sizes for two beam slices in multiple-slice model calculation of emittance compensation for 10-nC beam. A vertically focusing quadrupole is placed symmetrically over the cathode plane, followed by a horizontally focusing quadrupole, another doublet, a drift, and a TESLA cavity linac. (b) Vertical emittance evolution in this case.*

The polarized source cathode will need to be recesiated periodically and activated less occasionally. Both of these procedures are a threat to the required ultra-high-vacuum environment. A scheme involving a "loadlock" where the cathode can be retrieved and isolated from the gun vacuum environment to carry out these procedures needs to be incorporated into the gun design. Another possible option might be to mask the cathode with a "shroud" which is part of the cesiation or activation mechanism lowered directly into the gun. Further design studies to pin down the optimum way to carry out the cesiation and activation procedures is essential.

High-gradient Effects

The effects of high gradients in the vicinity of the GaAs cathode are best studied with a specially designed HIP copper rf gun whose design allows for a 42 $\ell/$s pumping speed. This design should incorporate an rf feed that will eliminate the dipole-field asymmetry and allow for the mechanical positioning of the emittance compensation magnet in its optimal position. The properties of the various cathode materials will detune

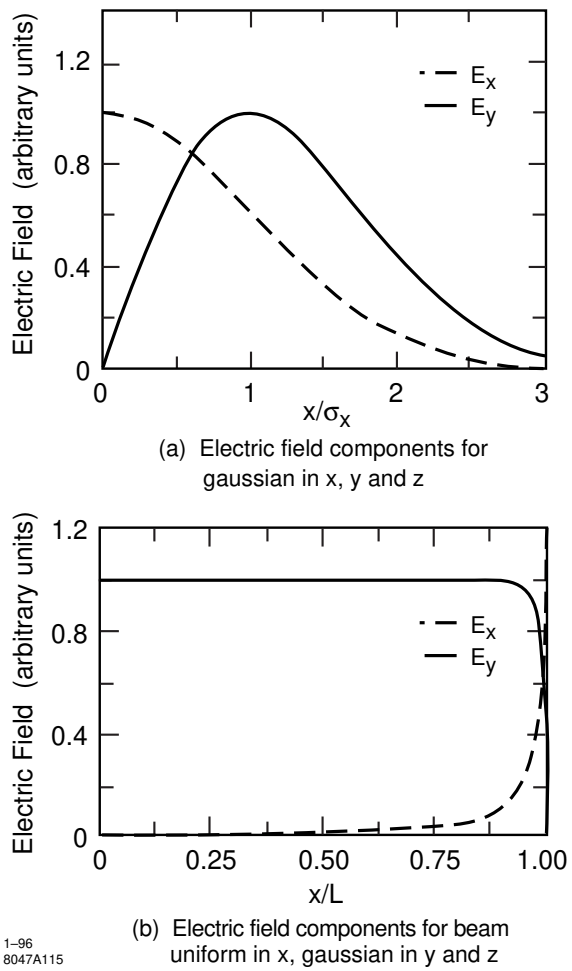

Figure 2-24. *Electric field components for (a) uniform, as opposed to (b) horizontally-Gaussian density profile.*

the half-cell resonant frequency and thereby effect the field balance of the gun. Symmetric tuners in both the full and half cell will be needed to maintain the $f_\pi = 2856\,\mathrm{MHz}$ with the interchange of different cathode material under ultra-high-vacuum conditions. Also, the field levels in the full and half cell will need to be monitored during operation. The mechanical and rf design of these coupling probes should not induce dipole asymmetries in the cavities which would cause emittance growth in the beam.

To maintain the high gradient in the gun necessary for the emittance compensation at S-band, the mechanical design should take into account the scheme discussed in Section 2.A.3, "Vacuum", for the recesiation process of NEA photocathode materials.

There is a plan to install a GaAs cathode from SLAC in the rf gun at CERN and to study survivability in the presence of rf. The success of this test would be important in building confidence in the feasibility of polarized-source rf guns, but failure would not necessarily rule out the possibility of using a polarized rf gun for the NLC since the CERN Linear Collider Test Facility (CLIC) gun is not specifically designed for this test.

It is important to pursue a dedicated effort to carry out the full measure of high-gradient studies at SLAC. This would entail the design and construction of a new rf gun which includes the necessary upgrades discussed above to make the present BNL/SLAC/UCLA 1.6-cell S-band rf gun a polarized electron source.

Photocathode Response Time

In order for an S-band rf gun to produce a beam with a bunch length that meets the NLC injector requirement, *i.e.,* not to exceed 20 ps in full pulse length, the response time of the photocathode must be $\leq$10 ps. For a thin strained GaAs photocathode whose surface is treated to have negative electron affinity, the photoemission response time is determined by the thickness of the active layer, which is typically 100 nm, and by the electron diffusion coefficient. With a doping density in the mid-10^{18}-cm^{-3} range, the diffusion coefficient in GaAs is about 35 cm^2/ at room temperature [Sze 1981], Thus, in the absence of multiple emission attempts, the response time for a 100-nm-thick cathode is estimated to be approximately 3 ps, which adequately meets the requirement for response time. However, this estimate ignores the likely scenario in which an excited electron may require several attempts to be emitted as it may fail to escape the first time or even the first few times it reaches the cathode surface and, as such, must be regarded as a lower limit on the response time. Electrons that are emitted after multiple escape attempts will ultimately lead to a longer response time and may prevent negative electron affinity photocathode from being incorporated into an S-band rf gun.

Measurements of the response time for GaAs photocathodes have been made only with bulk samples [Aleksandrov 1995, Hartmann 1995a]. Aleksandrov *et al.,* placed an upper limit of 40 ps on the response time, whereas Hartmann *et al.,* found it to be about 30 ps. However, both measurements were done under the condition that the cathodes' quantum efficiencies were more than an order of magnitude lower than that of an optimally activated bulk GaAs, implying that the essential property of negative electron affinity is or close to be lost. Therefore, the measured response time is actually that of a thin active emitting layer at the surface of the bulk GaAs cathode, whose thickness is probably on the order of 100 nm due to the lack of negative electron affinity, rather than that of the bulk GaAs cathode. In this sense, these two studies may represent an experimental approximation for measuring the response time of a 100 nm strained GaAs cathode. Of course, since the response time depends quadratically on the thickness of the active emitting layer and it is difficult to estimate its exact value given a bulk GaAs cathode with a low quantum efficiency, the measured response time should be regarded only as an order of magnitude estimate for a 100-nm strained GaAs cathode. Ultimately, the exact response time for such a cathode must be determined experimentally under a high quantum efficiency condition appropriate for high beam intensity operation. At present, it appears that the response time of such cathodes may marginally satisfy the requirement of an S-band rf gun.

Photocathode Charge Limit

For a thin strained GaAs photocathode to be used in an rf gun for NLC, it must be capable of producing up to 3 nC of charge for an approximately 20-ps-long bunch, which implies that the charge limit of the cathode for a 20 ps charge pulse needs to be $\geq$3 nC. Earlier charge limit studies at SLAC has shown that the cathode charge limit in a 2-ns pulse depends almost linearly on the cathode bias or equivalently the extraction electric field at the surface within a range from 0.15 to 1.8 MV/ m [Tang 1994a]. In an rf gun, the extraction field at the cathode surface is on the order of 100 MV/ m, which is about two orders of magnitude higher than that in an SLC polarized electron gun operated at 120 kV. If the linear scaling with respect to extraction field remains valid up to orders of magnitude higher fields, then, the charge limit of a similar cathode in an rf gun will be scaled higher by the same factor. The maximum observed charge limit for a 2-ns charge pulse from a 100-nm strained GaAs cathode with an 80% polarization in an SLC gun was about 9.5 nC/ cm^2 at an extraction field of 1.8 MV/ m. Scaling to 100 MV/ m yields the charge limit for a 2-ns pulse in the rf gun

to be about 530 nC/ cm^2. Based on the fact that the typical size of the laser beam used to illuminate the cathode in an S-band rf gun is 1-mm in radius, the maximum extractable charge from such a cathode for a 2-ns pulse is estimated to be approximately 17 nC.

It remains to estimate the charge limit in the rf gun for a 20-ps pulse. Unfortunately, no systematic studies on the effect of the pulse length, especially in the picosecond regime, on the charge limit have been made. Observation made during earlier R&D experiments of the SLAC polarized electron source has shown that the charge limit does depend, albeit not strongly, on the pulse length. For example, the charge limit for a 200-ns pulse was observed to be more than five times greater than that of a 2-ns pulse in an SLC gun. Physics consideration suggests that from 2 ns to shorter time scales the charge limit should depend on the pulse length more weakly. Thus, given the estimated charge limit of 17 nC in an rf gun for a 2-ns pulse, the prospect of achieving $\geq$3 nC in a 20-ps pulse appears reasonable. Plans have been made to systematically study this dependence for pulse lengths ranging from several nanoseconds to sub-nanosecond scales to further our understanding of this important issue. Finally, it is worth noting that the extremely high extraction field in an rf gun will greatly mitigate the multi-bunch effect of the charge limit phenomenon.

2.A.4 Laser System

Energy Requirements

The laser system for an rf gun for NLC, which is shown in Figure 2-25, must produce a train of 90 pulses separated by 1.4 ns, corresponding to a frequency of 714 MHz. This 126-ns pulse train (the macropulse) repeats at 180 Hz. Each of these 90 micropulses in the train must have a width adjustable between 5 and 20 ps, so that the emittance can be minimized. This optimization will also involve adjusting the temporal pulse shape (to be discussed below). Each pulse must be sufficiently intense to generate a charge of up to 4 nC (2.5×10^{10}) electrons. To obtain the high polarization (80%) now achieved with the SLC's DC cathode, a strained GaAs cathode would again be used, with an excitation wavelength near 850 nm. For this material and wavelength, a quantum efficiency of 0.1% has been measured in the DC gun. In an rf gun, the efficiency could be higher due to enhancement by the high rf electric field on the cathode, or lower if the rf causes degradation of the surface. Assuming $QE = 0.1\%$, the laser must produce a train of pulses on the cathode with at least six μJ/micropulse and 0.5 mJ for the macropulse. With a safety factor of eight to allow for losses in the optics and declines in quantum efficiency, the laser must be capable of delivering up to 4 mJ at the output of the laser pulse compressor over the 90-pulse train.

Stability Requirements

A high degree of stability in several laser parameters is essential for the NLC. Variations in the energy per pulse, both within one macropulse and from macropulse to macropulse, should be limited so that the charge per pulse is constant. Charge fluctuations vary the beam loading in the accelerator sections, and hence introduce additional energy spread in the beam. Allowable intensity jitter budgets are discussed in Chapter 1. The allowable macropulse charge intensity fluctuation needs to be less than 0.5% rms. Thus for the NLC, we require a variation of no more than 0.5% rms in the macropulse laser energy and in the overall flatness of the envelope of the micropulses in each macropulse. Fluctuations of 2% are tolerable from one micropulse to the next.

In an rf gun, the laser pulse must occupy a small fraction of the rf period, with typical widths of 10 to 15 ps. The laser's repetition frequency must be tightly locked to a subharmonic of the rf frequency. Pulse-to-pulse

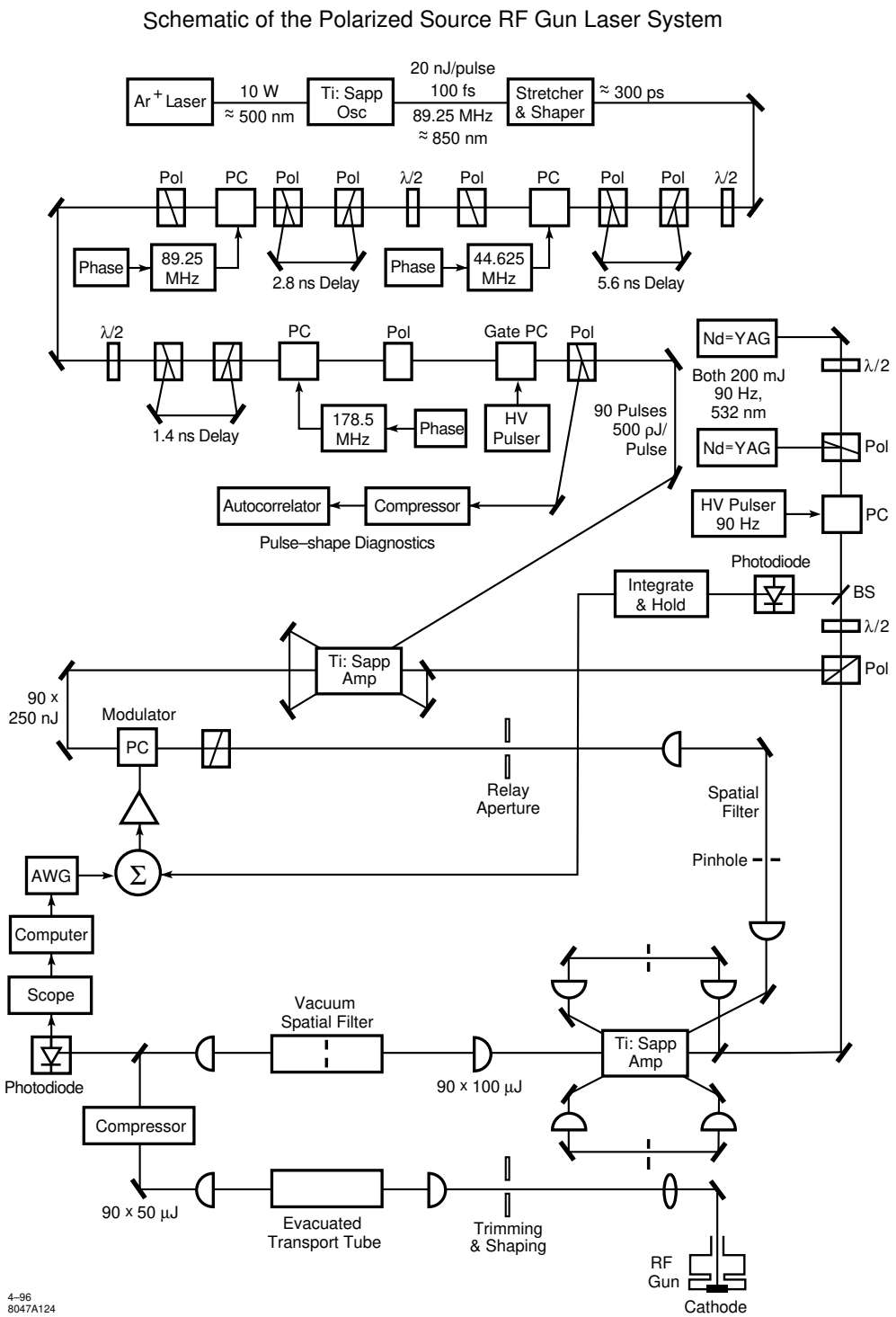

Figure 2-25. *Schematic diagram of the polarized-source rf gun laser system.*

timing jitter, with respect to the phase of the gun's rf, leads to energy changes and also affects the beam's transverse phase space. This jitter must be kept below 1 ps rms.

The goals also include 1% variations in the diameter of the laser spot on the photocathode, with a centroid location that varies by no more than 1% of the diameter. The micropulse duration should also fluctuate by no more than 1%. Techniques for achieving this stability will be discussed below.

Oscillator

A CW actively mode-locked oscillator is needed to obtain picosecond pulses synchronized with the rf. As with the DC gun's laser, titanium sapphire is a natural choice for this wavelength range. Commercial mode-locked Ti:sapphire oscillators are available with wide tunability (from 700 to 1060 nm), 1 to 2 W of output power, and, in some types, with pulse widths selectable from 0.1 to 60 ps. A 10-W CW argon-ion laser provides the pumping, and can be stabilized with feedback for both pump power and pointing. Compared to other oscillators (*e.g.,* Nd:YLF or Nd:YAG), it is difficult to lock Ti:sapphire oscillators to an external rf source, since they tend to self-mode-lock due to inherent nonlinearities, without any reference to an external drive. However, carefully timed feedback to adjust the cavity length can control both the mode-locking frequency and phase relative to the reference signal. The commercial products claim a timing jitter below 2-ps rms, but measurements of 1 ps have been made, approaching the best values obtained with Nd:YLF. However, these units support pulse trains at frequencies of about 80 to 100 MHz. A new design with an extremely short cavity would be needed to mode-lock at the 714 MHz required for the NLC.

It is possible to provide a higher pulse-train frequency while making use of a standard oscillator. Start with a linearly polarized laser operating in the commercial range, at 89.25 MHz, which is 1/8 of the desired frequency and corresponds to a pulse spacing of 11.2 ns. Split the beam in two with a half-wave plate and polarizer. Delay one beam by half the pulse spacing, 5.6 ns, which requires an additional path of 1.7 m. Recombine the beams with a second polarizer, then use a Pockels cell driven by rf at 44.6 MHz to restore all pulses in the train to the original polarization. By repeating this process two more times with delays of 2.8 and 1.4 ns, and with Pockels cells at 89.25 and 178.5 MHz, we can prepare a complete pulse train with the desired 1.4-ns spacing. At times, the NLC may be operated with micropulses spaced by 2.8 or 5.6 ns. The number of pulses would be reduced by the same factor, so that the macropulse duration remains fixed. These spacings are readily accomplished by rotating the waveplates at the third (and second, for the 5.6-ns case) splitting, so that no splitting takes place.

Efforts are also underway to develop a mode-locked Ti:sapphire oscillator with a pulse train repeating at a very high rate. Hartmann and colleagues [Hartmann 1995b] have built a 76.54-MHz Kerr-lens-mode-locked Ti:sapphire oscillator synchronized with an external rf source. They have presented preliminary results from a second oscillator with a repetition rate of 1.039 GHz; this frequency will next be raised to 1.225 GHz, and the eventual goal is 2.45 GHz. Even the demonstrated operating frequency is fast enough for the NLC, and such a laser would avoid the elaborate split-and-delay procedure of the previous paragraph.

Diode lasers may offer a promising alternative that can provide even lower jitter. Their small size makes them well suited for high repetition rates. They can be actively mode-locked with minimal jitter, since the laser gain can be directly modulated by applying an rf signal to the diode, without the need for an acousto-optic device to modulate the cavity Q. Diode lasers combining active and passive mode-locking have been developed [Delfyett 1992] at frequencies from 302 to 960 MHz, at wavelengths near 830 nm, and with bandwidths of 4–10 nm. When followed by another diode acting as an amplifier, and after removing the chirp, Fourier-transform-limited pulses of 0.46 ps with a jitter of 0.4 ps were obtained. These pulses can be dispersively stretched to any desired width while maintaining the low jitter. Filtering in the compressor removes unwanted spontaneous emission. However, compared to the Ti:sapphire oscillator, the output power

is low, typically 10 mW, and so more amplification would be needed. There is also considerably less tunability. This second drawback may not be too serious, since a diode laser could be prepared to operate at whatever wavelength proves best for the polarized rf gun. Wider micropulse spacings can be implemented by driving the diode laser directly at 357 or 178.5 MHz, so that the gain is high only at multiples of the fundamental cavity spacing. With further development, this source may be well suited to providing the high repetition rate and low jitter needed for NLC.

A4.4 Amplifier

With either oscillator, the amplifier is similar to that proposed for the laser system for the NLC's DC gun—a multiple-pass Ti:sapphire amplifier pumped by two *Infinity* Nd:YAG lasers from Coherent Inc., each providing 200 mJ at 532 nm in alternation at 90 Hz. However, the pulsed oscillator used with the DC gun produces 100 nJ in each micropulse, after allowing for the losses in the Pockels cells that shape its train of square, 1-ns-wide pulses. This is more energy than is produced by either type of CW mode-locked oscillator. Consequently, we need more amplifier gain, which can be obtained with two amplifier stages, with the pump light split between them. With the Ti:sapphire oscillator, the 3-pass bowtie configuration with a gain of 8 to 10 per pass, would be suitable for both stages. For the diode laser, where the energy extraction would be very low in the first pass, a 5-pass first stage and a 3-pass second stage would provide sufficient gain.

Fourier-Relay Optics

A technique known as Fourier relay optics can address the conflict between two important goals: better energy extraction by filling the rod more completely, while maintaining a clean transverse mode. Initially, the oscillator beam is trimmed in an aperture. The technique combines relay imaging, in which lenses relay an image of this aperture to each pass through an amplifier rod, and filtering of the beam's spatial Fourier transform. At each step, a lens of focal length f_1 is placed a distance f_1 after one of the image planes. The Fourier transform is formed at the focus, f_1 beyond the lens, where higher spatial harmonics are removed by a pinhole. A second lens with focal length f_2 then recollimates the beam (with expansion $\frac{f_2}{f_1}$) and forms the relay image at a distance $f_1 + f_2$ from the previous image plane. An image of the aperture is finally relayed to the photocathode, to define the area of photoemission.

Shaping the Beam in Space

We usually consider laser pulses that are Gaussian in time and space. However, it would be useful to investigate ways of making electron pulses that are more square, with steeper sides and flatter tops. Simulations of Brookhaven's rf electron gun have shown that electrons emitted during the temporal tails of a Gaussian laser pulse occupy a different region of phase space than those emitted near the middle. With a flatter laser pulse, the electrons are more tightly clustered, with a lower emittance over the full pulse (although the instantaneous "slice" emittance at times within the pulse is similar). Calculations also show that flattops in both space and time are best for emittance compensation using solenoidal focusing after the gun.

To shape the pulse in space, a position-dependent attenuation could be applied to the beam [Van Wonterghem 1993]. Relay imaging should be used after the flattening, to limit diffraction. Stability of the laser's position and diameter on the photocathode can be achieved by trimming the edge of the beam with an aperture on the final relay plane; this aperture is then imaged onto the photocathode. While a Gaussian beam could still have fluctuations in the position of the centroid within the aperture, with a flattop beam, pointing jitter does not cause any change in cathode illumination.

An rf gun that directly produces a spatially flat electron beam is under consideration. The flat-beam gun would have a vertical beam size and emittance substantially smaller than the horizontal, as ultimately required at the interaction point. The required flat laser pulse can readily be produced with a small modification of the final relay stage: a pair of cylindrical lenses could provide different magnifications in the two transverse directions to produce an ellipse on the cathode.

Stretching, Compressing, and Shaping the Micropulses in Time

In amplifiers for picosecond and especially subpicosecond pulses, the peak power must be limited to avoid optical damage and nonlinearities. The Ti:sapphire oscillator can produce a 0.1-ps pulse with a large bandwidth. The dispersion of a grating pair can then stretch the pulse to hundreds of picoseconds, so that the peak power is reduced before amplification. The stretching results from having different wavelengths in the pulse take different optical paths, and so correlating time, space, and wavelength. After amplification, the process can be reversed to compress the pulse to the original or any greater width. This technique is known as chirped-pulse amplification [Maine 1988].

During the stretching, temporal pulse shaping is readily accomplished in the dispersive region between the gratings, by using a spatially varying filter to selectively attenuate the wavelengths corresponding to different times [Skupsky 1993]. (Filtering could also be done in the compressor, but the power levels are higher.) More sophisticated shaping, including the production of square picosecond pulses, has been achieved using both amplitude and phase masks to manipulate the pulse's Fourier transform [Weiner 1988]. The rise time and flatness of the resulting pulse are limited by the bandwidth of the input pulse, determined by the oscillator's pulse width. Thus the shaped pulse cannot rise faster than the oscillator.

For lower-resolution shaping, an interesting possibility is the use of a linear array of liquid crystals to form a voltage-controlled, spatially varying, amplitude mask, allowing active control of the pulse shape. Guided by measurements of the amplified pulse shape, a computer could provide a feed forward, adaptive control system.

Pulse-width stability is important for the NLC's performance. If the bandwidth of the oscillator pulse is wider than that transmitted by the phase and amplitude masks, so that the masks are illuminated almost uniformly, then fluctuations in the oscillator width do not affect the final pulse width or shape, which is determined only by the masks and the pulse compressor following the amplifiers.

Feedback and Feed-Forward Corrections

A high-extinction (>1000), fast-rise, variable-width, Pockels-cell gate after the oscillator chops the pulse train to the desired length. Over the course of the macropulse, a substantial fraction of the energy stored in the amplifiers by the pump laser is extracted. To compensate for the resulting drop in gain for the later micropulses, a second Pockels cell after the oscillator or between the amplifiers modulates the macropulse, attenuating the early pulses to flatten the envelope of the pulse train. An arbitrary waveform generator drives the Pockels cell with a waveform that results in a flat pulse train after amplification. A computer controls the process in a feed-forward loop: the computer monitors the envelope with a photodiode and continually reprograms the arbitrary waveform generator for subsequent macropulses to maintain the desired envelope.

For modulation, it is convenient to use a cell that imposes a transverse field across a crystal such as Lithium Tantalate (LTA). Although the extinction is not as high as that of the more common, longitudinal-field, Dereterated Potassium Dihydrogen Phosphate (KD*P) cell used for the gate, the switching voltage is much lower—about 150 V rather than 8000 V for half-wave rotation. The difficulty of making a high-voltage,

high-speed, linear amplifier is avoided; instead, a transverse-field cell is available from Conoptics matched to a 120-MHz solid-state linear amplifier. The high bandwidth of the driver, and its 1-V input, allow for sophisticated control of the macropulse envelope.

Feed-forward should compensate well for droop and slow drifts in the laser's performance. Random, shot-to-shot fluctuations will also arise, largely due to fluctuations in the flash lamps of the pump laser. Feedback within each macropulse is needed to correct for shot-to-shot changes in the envelope. An error signal for feedback could be made by comparing the measured envelope to a square pulse. This difference could then be subtracted from the arbitrary waveform generator output. However, cable delays and the amplifier's internal propagation delay limit the feedback bandwidth to about 3 MHz. In principle, the amplified pulses could be measured, then delayed with several meters of optical path while the voltage on a Pockels cell is adjusted. Fast and precise electronics would be required to achieve the desired accuracy. Such a correction has been tried briefly on the SLC's gun laser, but noise in the electronics limited the correction to about 2%.

Other approaches are more practical. We could monitor the pump energy and derive a correction added to the arbitrary waveform generator output over the macropulse. Since the *Infinity* pump laser has a pulse duration of 3.5 ns and titanium-sapphire has an upper-state lifetime of 3 μs, there is sufficient time between pumping and extracting to make this correction. Alternatively, we could widen the gate, then use the modulator Pockels cell to shape the pulses into two trains separated by about 1 μs. After amplification, the earlier one, occurring after the rods are pumped but before the gun's rf starts, would be measured to sense the system gain. The later pulse could then be corrected and sent to the gun.

2.A.5 Integrated System

Once the various physics issues and technical difficulties have been resolved for the polarized source photocathode rf guns, an integrated system including the laser and accelerator beam line up to 80 MeV needs to be constructed and demonstrated to operate in a stable, reliable, and efficient way, for an extended period of time. When the system integration tests show that a polarized photocathode rf gun can operate with a 99% availability, it will become the most attractive option as an injector the NLC.

2.A.6 Conclusions

The polarized source photocathode rf gun is a significant option for the NLC injector because of the potential of producing low emittance bunch trains from the injector region, thus simplifying the design of the damping ring or at least simplifying the operation of the damping ring. If the various physics issues concerning the beam dynamics and the technology issues of reliable operation of a polarized source rf gun are solved in the laboratory, it would become the most attractive option for the polarized electron source for the NLC.

2.B Charge Limit and its Implications on High-Polarization Long-Pulse Charge Production

2.B.1 Introduction

The charge limit (CL) phenomenon refers to the suppressed emission of excited electrons in the conduction band from a p-type negative electron affinity (NEA) or nearly NEA semiconductor cathode due to an increase in the surface work function caused by those electrons that fail to escape and eventually become trapped at the surface [Woods 1993]. This happens because among the largely thermalized conduction band electrons that reach the surface, only a fraction of them may successfully escape due to limited escape probability as determined by the surface NEA property. The electrons trapped at the surface are removed mainly by combining with holes that tunnel to the surface through the band-bending potential barrier at a rate critically dependent on the doping density [Tang 1994b]. Charge limit (CL), or suppressed emission, occurs only if the excitation laser intensity is sufficiently high such that the rate of electrons getting trapped at the surface considerably exceeds the rate of removal and, therefore, leads to an appreciable buildup of electrons at the surface within the laser pulse duration. CL is not a total charge limit, as was originally believed. In a long-pulse mode, CL will likely manifest itself as a current limit. CL depends on the extraction electric field, in this respect bearing a vague resemblance to the space-charge limit, as well as on the cathode's quantum efficiency (QE) [Tang 1993]. The significance of the CL effect with respect to high-current long-pulse charge production is well addressed in reference [Tang 1994c].

In the summer of 1993, a systematic experimental study on the CL phenomenon using a series of strained layer GaAs cathodes was conducted. The cathodes used in that study included 100-nm and 300-nm high- and medium-doping (2×10^{19} and 5×10^{18} cm^{-3}, respectively) strained GaAs, etc.. It is fair to state that from this study most of the important properties of the CL phenomenon for 2-ns pulses were learned. These results may be used to project the CL behavior for long-pulse ($\sim$100-ns) operations before actual long-pulse CL data become available. Reference [Tang 1994c] furnishes a quantitative analysis of the prospects of producing the required charge from a polarized electron photocathode for the NLC using the 300-nm medium- and high-doping strained GaAs cathodes used in the 1993 study. The conclusion was that charge production for the NLC appears possible only with the high-doping cathode. The fundamental deficiency associated with the medium-doping cathode was its long relaxation time of the bunch-bunch effect, which leads to a substantial increase in the surface work function and, therefore, strongly suppressed emission in the high-current long-pulse operation required by the NLC.

2.B.2 Generalization of CL Effect to Long-Pulse Operation

In the following, a similar long-pulse CL analysis as presented in reference [Tang 1994c] shall be given for a 100-nm high-doping strained GaAs cathode, also used in the 1993 study. When excited at the band-gap threshold, that is, at 866 nm, this cathode yielded a maximum polarization for emitted electrons of about 65%. The relevant experimental 2-ns CL data from this cathode are shown in Figures 2-26 and 2-27. For the sake of facilitating our quantitative analysis, it will be assumed that a 866-nm laser pulse with a sufficiently long, flattop pulse length (>126 ns) is used to illuminate the cathode. Under the illumination of the long laser pulse, the cathode response will first undergo a transient period during which the photocurrent yield will vary (or more exactly, decrease) with time. The duration of the transient period will be determined by the relaxation time of the bunch-bunch effect and the instantaneous laser power within the pulse. A steady

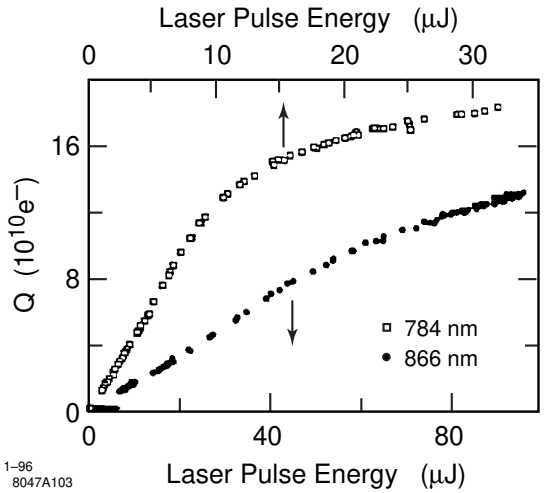

Figure 2-26. *Change vs. laser pulse energy for a 100-nm high-doping strained GaAs cathode with $QE = 22\%$ measure at 833 nm. The cathode is biased at 120 kV. Note that charge saturation was not reached at 866 nm due to insufficient laser energy.*

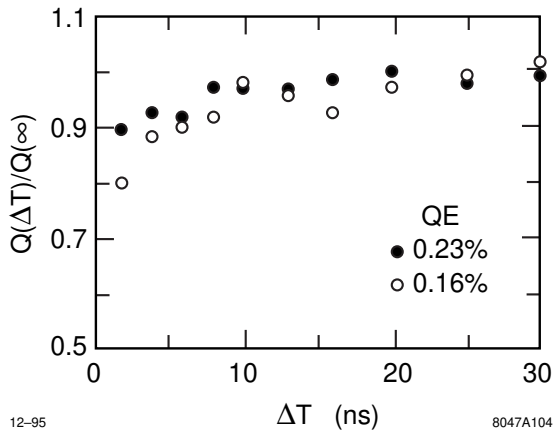

Figure 2-27. *Bunch-bunch effect for a 100-nm 2×10^{19} cm^{-3} doped strained GaAs sample for two different QE conditions (measured at 833 nm). Bunch 2 is at peak polarization with a laser pulse energy of 95 μJ at 866 nm. Laser pulse 1 is at 784 nm and has 32 μJ.*

emission state will be realized following this initial transient period. It is this steady-state emission current that we will try to evaluate based on the available 2-ns charge pulse data.

Based on the earlier assumption that the beam from the gun is a long 126-ns square pulse, we need a steady-state emission of roughly 4 A from the cathode to meet the NLC Phase I requirement. We may view the long pulse as consisting of many back-to-back 2-ns pulses of 5×10^{10} electrons each. As shown in Figure 2-27, the bunch-bunch effect is almost completely diminished after 10 ns. Therefore, the emission of an arbitrary 2-ns pulse can be affected only by the five preceding 2-ns pulses. From Figure 2-26 we can see that a laser pulse of about 30 μJ at 866 nm, or about 5 μJ at 784 nm, is needed to produce a single stand-alone 2-ns pulse of 5×10^{10} electrons at $QE(833\,\text{nm}) = 0.22\%$ (slightly below the cathode's maximum QE of 0.23%). Neglecting the inter bunch effect, the total laser energy for five such pulses is 150 μJ at 866 nm or 25 μJ at

784 nm, which is less than the Bunch 1 laser energy used for taking the inter-bunch effect data shown in Figure 2-27 Here, the fact that Bunch 1 is at 786 nm hardly matters at all because the first bunch serves to pump a large number of electrons into the conduction band, thus saturating the cathode surface with electrons, and photoexcitation at 786 nm is about six times as efficient as at 866 nm for the cathode under study. Due to the accumulated electrons at the surface, the emission factor for the next pulse following these five pulses is reduced to about 0.9, corresponding to the first data point in Figure 2-27 for which Bunch 2 immediately follows Bunch 1 with a QE of 0.23%. This is a conservative estimate since it has been assumed that practically none of the electrons trapped at the surface during the five preceding pulses has been removed. Due to this interbunch CL effect, the actual laser energy required to produce a long pulse of intensity 5×10^{10} electrons per 2 ns needs to be about 10% higher. We can carry out the above sequence of analysis all over again with the upward-adjusted laser energy. Clearly, with a laser power of 15 kW($= 30\,\mu$J/2 ns) at 866 nm this cathode appears capable of producing the required 4-A-long pulse, with considerable headroom by noting that increasing the laser power would lead to an increased current up to a certain limit. Of course, overdriving the cathode with too much laser power would result in a decreased emission current due to overly suppressed emission. Even when the QE drops to 0.16%, this cathode still appears promising for generating the required 4-A steady-emission charge pulse.

In the NLC polarized electron source design, the long laser pulse that illuminates the cathode is actually modulated at a duty factor of 50% with a period of 1.4 ns. With such a modulated pulse, the charge buildup at the cathode surface that causes the charge limit effect will be reduced by a factor of two compared with a square pulse as assumed for the above analysis. This would allow us to double the instantaneous laser power in the modulated pulse while keeping the emission factor at a similar value and, therefore, lead to a factor of two increase in the instantaneous emission current in the steady emission state. Based on the above analysis, the 100-nm high-doping strained GaAs cathode appears capable of generating an 8-A instantaneous current in a 50% modulated pulse, which corresponds to a microbunch charge of 3.5×10^{10} electrons. Such charge performance should even be adequate for the 1.5 GeV NLC.

It must be stressed that the favorable conclusions obtained from this analysis and from reference [Tang 1994c] do not mean that high-doping cathodes are actually capable of generating NLC-type charge pulses. These analysis should be viewed as merely a logical and physically reasonable generalization of the CL effect from a nanosecond scale to a time scale of an order (or two orders) of magnitude greater. It is possible that new unknown CL properties may exist on such a long time scale which may adversely affect emission. Therefore, the ultimate proof must come from experiments.

2.B.3 Where We Are

Even if high-doping strained GaAs cathodes are indeed adequate with respect to charge production, they still suffer from the deficiency of lower polarization than their medium-doping counterparts. The highest polarization from a high-doping strained cathode is about 65% (with a 100-nm-thick active layer), which is substantially lower than the 80% polarization specified for the NLC. While medium-doping 100-nm strained GaAs cathodes, such as the ones used for E-143 and SLC94-95, meet the NLC polarization requirement, their long CL relaxation times severely limit their long-pulse charge production capability. Recent long-pulse charge tests using such a 100-nm strained GaAs cathode showed that these cathodes are capable of sustaining an emission current of about 0.7 A with an 80% polarization in an SLC gun. If, as proposed in the ZDR, a modulated laser pulse with a 1.4-ns period and a 50% duty factor within the pulse duration is used instead of the square laser pulse used in the test, the steady-state emission current within a microbunch should exceed 1 A, yielding a microbunch charge of $\geq 0.45 \times 10^{10}$ electrons. This leaves us about a factor of 4 (or 7) away

from realizing an NLC-I (or NLC-II) polarized electron source. While the difference is still substantial, an NLC source is certainly within reach.

2.B.4 Cathode Improvements and Outlook

The key to realizing an NLC source is improved cathode performance. Strained GaAs cathodes with a thickness on the order of 100 nm will be our primary choice because of their proven superiority in polarization performance. The 100-nm medium-doping strained GaAs currently used at SLAC may be improved via the following approaches:

1. Modulated cathode doping scheme: High doping (2×10^{19} cm^{-3}) in a thin, typically 10-nm, surface layer and low doping ($\leq 1\times10^{18}$ cm^{-3}) in the rest of the active layer. The high doping at the surface helps minimize the CL relaxation time, thereby enhancing the long-pulse current, whereas the low doping in the interior maximizes the electron polarization. The presently employed heat-cleaning method for NEA activation may not be compatible with such a cathode as it may destroy its modulated doping profile. Alternative cathode cleaning techniques, notably atomic hydrogen assisted low-temperature cleaning, will be investigated.

2. Cathode surface protection: As (Arsenic) capping. By growing an As cap layer of about 1-μm thick on strained GaAs before exposing to atmosphere, the active emission surface may be kept atomically clean. Such a clean surface may substantially improve the quality of an NEA activation. As a result, the cathode's quantum efficiency may be improved by about a factor of two. Such an improvement is expected to greatly suppress the CL effect, thereby maximizing the charge performance. As-capping is particularly desirable on modulated-doping cathodes since surface cleaning may be adequately performed at 400°C, which would leave the modulated doping profile intact, instead of at 600°C necessary for an uncapped cathode. The reduced heat cleaning temperature should also significantly improve the operational reliability of the loadlock system.

Other R&D areas on cathodes include tailoring the composition of both the substrate and the strained active layer to optimize the polarization and charge performances, and developing other types of cathode structures such as unstrained or strained superlattice cathodes.

At present, the Gun Test Lab and the Cathode Test Lab at SLAC are adequately equipped for polarization and 2-ns pulse charge tests. As new cathode materials arrive, such tests may be performed and the results may be used to project their long-pulse behavior. For actual NLC-type long-pulse tests, a high-powered long-pulse laser, such as the one discussed in Section 2.3 or a Q-switched flashlamp-pumped Ti:sapphire, must be developed.

In conclusion, the CL effect is the fundamental limiting factor for developing an NLC polarized electron source. The present SLC source is already within an order of magnitude in terms of charge performance from the ultimate NLC-III source. With the numerous possibilities of cathode improvements, however, the prospects for realizing an NLC source are very good. We should all be encouraged by the superb charge performance demonstrated by an As-capped KEK superlattice cathode [Kurihara 1995].

References

[Aleksandrov 1995] A.V. Aleksandrov *et al., Phys. Rev. E* **51**, 1449 (1995).

[Alley 1994] R. Alley *et al.,* "The Stanford Accelerator Polarized Electron Source", SLAC–PUB–95–6489 (1994).

[Alley 1995] R. Alley *et al.,* "The Stanford Linear Accelerator Polarized Electron Source", NIM in Physics Research, A365, 1–27 (1995).

[Carlsten 1989] B.E. Carlsten, *Nucl. Instr. and Methods* **A285**, 313 (1989).

[Clendenin] J. Clendenin *et al.,* "Prospects for Generating Polarized Electron Beams for a Linear Collider using an RF Gun", SLAC–PUB–6172.

[Delfyett 1992] P.J. Delfyett *et al., IEEE J. Quantum Electron.* **28**, 2203 (1992)

[Gallardo 1993] J.C. Gallardo and H.Kirk, "An Injection Scheme for the Brookhaven ATF Utilizing Space-Charge Emittance Growth Compensation", *Proc. 1993 Part. Acc. Conf.*, 3615–3617 (1993).

[Hartmann 1995a] P. Hartmann *et al.,* "Generation of short electron bunches from GaAs photocathodes", presented at the Workshop on Experiences with Polarized Electron Sources using GaAs Technology, Bonn, Germany (1995).

[Hartmann 1995b] P. Hartmann *et al.,* "Experience with Polarized Electron Sources using GaAs Technology", poster presented at Univ. of Bonn, Germany (June 10, 1995).

[Herrera-Gomez 1993] A. Herrera-Gomez, and W.E. Spicer, "Physics of high-intensity nanosecond electron source", *SPIE Proceeding Series*, **2022**, 51 (1993).

[James 1981] M. B. James, R. H. Miller, "A High Current Injector for the Proposed SLAC Linear Collider", *IEEE Trans. Nucl. Sci.* NS-28, (3), 3461, (1981).

[Kim 1989] K.J. Kim, *Nucl. Instr. and Methods* **A275**, 201-218 (1989).

[Kirk 1995] H. Kirk *et al., Proc. 1995 Part. Acc. Conf.*, 265 (1995).

[Koechner 1992] Walter Koechner, *Solid State Laser Engineering*, Springer Series, NY, 1992.

[Kurihara 1995] Y. Kurihara *et al.,* "A high polarization and high quantum efficiency photocathode using a GaAs-AlGaAs superlattice", *Jpn. J. Appl. Phys.*, **32**, 1837 (1995).

[Maine 1988] P. Maine *et al., IEEE J. Quantum Electron.* **QE-24**, 398 (1988).

[Matsumoto 1994] H. Matsumoto *et al.,* "High Power test of a High Gradient S-band Accelerator Unit for the Accelerator Test Facility", *Proc. LINAC 94*, 302–304 (1994).

[Naito 1994] T. Naito *et al.,* "Multi-Bunch Beam with Thermionic Gun for ATF", *Proc. LINAC 94*, 375 (1994).

[Palmer priv] D.T. Palmer, private communication.

[Palmer 1995a] D.T. Palmer *et al.,* TESLA FEL Group Meeting, August 1995.

[Palmer 1995b] D.T. Palmer *et al.,* "Simulation of the BNL/SLAC/UCLA 1.6 Cell Emittance Compensated Photocathode RF Gun Low Energy Beam Line", *Proc. 1993 Part. Acc. Conf.* (1995).

[Rosenzweig 1993] J.B. Rosenzweig and E. Colby, "Design of a High Duty Cycle, Asymmetric Emittance RF Photocathode Injector for Linear Collider Applications", *Proc. 1993 Part. Acc. Conf.*, 3021–3023 (1993).

[Rosenzweig 1995] J.B. Rosenzweig and E. Colby, "Charge and Wavelength Scaling of RF Photo Injector Designs", Advanced Accelerator Concepts (AIP Conf. Proc. 335) 724 (AIP, NY, 1995).

[Sheffield 1992] R.L. Sheffield *et al., Nucl. Instr. and Methods* **A318**, 282–289 (1992).

[Sheffield 1993] R.L. Sheffield *et al.,* "Operation of the High Brightness LINAC for the Advanced Free-Electron Laser Initiative at Los Alamos", *Proc. 1993 Part. Acc. Confl*, 2970–2972 (1993).

[Schultz 1992] D. Schultz *et al.,* "The Polarized Electron Source Performance in 1992 for SLC-SLD", presented at the Tenth Int. Sym. on H.E. Spin Physics, Nagoya (Nov. 9–14, 1992).

[Serafini 1995] L. Serafini and J.B. Rosenzweig, "Envelope Analysis of Intense Relativistic Quasi-laminar Beams in High Gradient Linacs", Submitted to *Phys. Rev. E* (1995).

[Skupsky 1993] S. Skupsky *et al., J. Appl. Phys.* **73**, 2678 (1993).

[Sze 1981] S.M. Sze, *Physics of Semiconductor Devices*, 2nd edition (John Wiley & Sons, NY, 1981).

[Tang 1993] H. Tang *et al.,* "Study of non-linear photoemission effects in III-V semiconductors", *Proc. 1993 Part. Acc. Conf.*, Washington DC, 3036 (1993).

[Tang 1994a] H. Tang *et al., Proc. Fourth European Part. Acc. Conf.*, 46 (1994).

[Tang 1994b] H. Tang *et al.,* "Experimental studies of the charge limit phenomenon in NEA GaAs Photocathodes", *Proc. Fourth European Part. Acc. Conf.*, London, England, 46 (1994).

[Tang 1994c] H. Tang *et al.,* "Prospects for a polarized electron source for next generation linear colliders based on a SLC-type gun", Proc. of the 11th Intern. Symp. on High Energy Spin Phys. (Bloomington, IN, 1994, in print).

[TESLA FEL] TESLA FEL Collaboration, TESLA-FEL 95-03.

[Travier 1994] C. Travier, "Review of Electron Guns", *Proc. EPAC94*, 317–321 (1994).

[Van Wonterghem 1993] B.M. Van Wonterghem *et al.,* Proc. Conf. Laser Coherence Control, SPIE Vol. **1870**, 64 (21–22 Jan. 1993).

[Wanant 1994] R. Waynant, M. Ediger, *Electro-optics Handbook*, Optical and Electro-optical Engineering Series, 34 (McGraw-Hill, 1994).

[Weiner 1988] A.M. Weiner *et al., J. Opt. Soc. Am.* **B5**, 1563 (1988).

[Woods 1993] M. Woods *et al.,* "Observation of a charge limit for semiconductor photocathodes", *J. Appl. Phys.* **73**, 8531 (1993).

[Yoshioka 1994] M. Yoshioka *et al.,* "High Gradient Studies on UHV Room Temperature Cavities at S-Band for Linear Colliders", *Proc. LINAC 94*, 302–304 (1994).

Contributors

- Ray Alley
- David Burke
- Jym Clendenin
- David Farkas
- Allan Fisher
- Joseph Frisch
- Zhenghai Li
- Roger Miller
- Yuri Nosochkov
- Dennis Palmer
- Tor Raubenheimer
- Louis Rinolfi
- James Rosenzweig
- Huan Tang
- Kathy Thompson
- James Turner
- A. Dian Yeremian
- Dieter Walz
- Juwen Wang